

Theoretical study of mixing in liquid clouds. Part 1: classical concepts

(revised version, 14 March 2016)

Alexei Korolev¹, Alex Khain², Mark Pinsky², and Jeffrey French³

[1] Environment Canada, Cloud Physics and Severe Weather Section, Toronto, Canada

[2] Department of Atmospheric Sciences, the Hebrew University of Jerusalem, Israel

[3] University of Wyoming, Laramie, WY, USA

Correspondence to: A. Korolev (alexei.korolev@canada.ca)

Abstract

The present study considers final stages of in-cloud mixing in the framework of classical concept of homogeneous and extreme inhomogeneous mixing. Simple analytical relationships between basic microphysical parameters were obtained for homogeneous and extreme inhomogeneous mixing based on the adiabatic consideration. It was demonstrated that during homogeneous mixing the functional relationships between the moments of the droplets size distribution hold only during primary stage of mixing. Subsequent random mixing between already mixed parcels and undiluted cloud parcels breaks these relationships. However, during extreme inhomogeneous mixing the functional relationships between the microphysical parameters hold both for primary and subsequent mixing. The obtained relationships can be used to identify the type of mixing from in situ observations. The effectiveness of the developed method was demonstrated using in-situ data collected in convective clouds. It was found that for the specific set of in-situ measurements the interaction between cloudy and entrained environments was dominated by extreme inhomogeneous mixing.

1 Introduction

Turbulent mixing is an important non-adiabatic process in the atmosphere that to a large extent determines spatial gradients of many thermodynamic (e.g. temperature, humidity) and cloud microphysical parameters (e.g. hydrometeor concentrations, extinction coefficient, condensed water content) and as such, needs to be properly described in numerical simulations of clouds and weather predictions. Entrainment and mixing occurs during the entire lifetime of a cloud and is active not only near cloud edges, but it is important throughout the whole cloud volume. Mixing of cloudy and entrained air results in changes to the shape of the droplet size distribution through partial droplet evaporation and can also lead to changes in droplet concentration through complete evaporation of some fraction of droplets and dilution. The shape of the droplet size distribution plays key role in the initiation of precipitation and radiative properties of clouds.

The treatment of mixing in numerical simulations of clouds and precipitation formation remains a challenging problem. Besides the issues related to the way to describe mixing in numerical schemes, there is a fundamental problem of identifying a scenario or path, that mixing events should follow. Through the pioneering works of Latham and Reed (1977) and Baker et al. (1980) two explicitly alternative scenarios of mixing were identified. In the first scenario turbulent mixing rapidly stirs the environment homogenizing the fields of temperature and humidity. Following that, all of the droplets undergo partial evaporation under the same conditions. The result of this mixing is a droplet population with reduced sizes, but a total number that remains unchanged. This type of mixing is referred to as *homogeneous*. In the second scenario mixing occurs more slowly such that the population of droplets experiences different amount of sub-saturation. Some number of droplets completely evaporates, while others experience no evaporation until the entirety of the entrained air becomes saturated. Following that, turbulence mixes the rest of the droplets with the saturated, but droplet-free environment. During this type of mixing the size of droplets remains unchanged; however, their total number is reduced. This type of mixing is called *extreme inhomogeneous*. The intermediate case when some fraction of droplets evaporates partially, another other fraction evaporates completely, and a third fraction remains unchanged is in some works referred to as inhomogeneous (e.g. Baker and Latham, 1980).

The conditions for homogeneous and extreme inhomogeneous mixing and their effects on precipitation formation have been debated in cloud physics over forty years. There are a number of numerical simulations and theoretical efforts on studying different aspects of mixing and its effect

63 on cloud microphysics (e.g. Baker and Latham, 1982; Jensen and Baker, 1989; Su et al., 1989;
64 Lasher-Trapp et al., 2005; Jeffrey, 2007; Andrejczuk et al., 2009; Kumar et al., 2013; Jarecka et al.
65 2013 and many others). A comprehensive review of the works on the effect of turbulence and
66 mixing on cloud droplet formation can be found in Devenish et al. (2012).

67 A number of studies were dedicated to identifying type of mixing based on in-situ
68 observations. Most of the previous observations provided evidence supporting inhomogeneous
69 mixing (e.g. Hill and Choulaton, 1985; Paluch, 1986; Bower and Choulaton, 1988; Blyth and
70 Latham, 1991; Gerber et al., 2008, Lu et al. 2011; Beals et al. 2016). However, works of Jensen
71 and Baker (1989), Paluch and Baumgardner (1989), Burnet and Brenguier (2007), Lehmann et al.
72 (2009), Lu et al. (2011) suggested occurrence of homogeneous mixing. So, at the moment it
73 appears that both types of mixing may occur in liquid clouds. However, the environmental
74 conditions governing one or the other type of mixing remain not well understood.

75 Early experimental work on identifying type of mixing from in-situ observations were based
76 on the analysis of spatial variability of the shapes of individual droplet size distributions (e.g.
77 Paluch and Knight, 1984; Paluch, 1986; Bower and Choulaton, 1988). The effectiveness of this
78 method involving the analysis of a large number of individual size spectra turned out to be quite
79 low. Another technique utilized expected functional relationships between droplet concentration
80 (N) and droplet diameter (D) specific to each type of mixing. Thus, during extreme inhomogeneous
81 mixing the droplet size is expected to remain unchanged, whereas the concentration will vary.
82 During homogeneous mixing the droplet size and concentration in cloud will be related to each
83 other in a certain way, depending on the mixing fraction and the humidity of the entrained air. This
84 fact was used in observational studies for identifying the type of mixing from “mixing diagrams”
85 that related N and D_v for different regimes of mixing (e.g. Burnet and Brenguier, 2007; Gerber et
86 al., 2008; Lehmann et al., 2009).

87 The use of mixing diagrams to some extent facilitated identification of type of mixing.
88 However, in many cases scatter in the relationships between N vs. D_v was too large, hindering
89 identification of the type of mixing (Burnet and Brenguier, 2007). To resolve this problem many
90 researchers used other complementary measurements supporting identification of the type of
91 mixing (e.g. Gerber et al., 2008; Lehmann et al., 2009).

92 Besides the effect on N and D_v , the type of mixing is anticipated to manifest itself in
93 relationships between other moments of the droplet size distribution, $f(D)$. Such relationships may

94 provide insight into the mixing process and identify type of mixing. With the exception of the work
95 by Hill and Choullarton (1985), who correlated concentration and liquid water content, there have
96 been few attempts to use any other microphysical parameters for identification of type of mixing.

97 In order to fill this gap, this study presents a theoretical analysis of relationships between
98 different moments of $f(D)$ within the framework of homogeneous and extreme inhomogeneous
99 mixing. The analysis is focused on the first four moments of $f(D)$ corresponding to the droplet
100 concentration N (0th moment), integral diameter $N\bar{D}$ (1st moment), extinction coefficient β (2nd
101 moment), liquid water mixing ratio q (3rd moment) and mean volume diameter D_v (mixed 3rd and
102 0th moment). It is shown that the newly obtained relationships between the moments provide a
103 more robust identification of type of mixing from in-situ measurements as compared to
104 conventional $N - D_v^3$ relationships used in mixing diagrams. Relationships between moments may
105 be useful for parameterization of mixing in numerical simulations of clouds and climate,
106 interpretations of remote sensing measurements.

107 This paper constitutes the first in a series of three papers. It considers the final stage of mixing
108 based on the formal definitions of homogeneous and extreme inhomogeneous mixing. These two
109 types of mixing present two extreme regimes of mixing. The following two papers provide a
110 detailed analysis of the time dependent processes during homogeneous (Pinsky et al., 2015a) and
111 inhomogeneous (Pinsky et al., 2015b) mixing where non-extreme regimes are considered as well.

112 This paper is arranged in the following way. Section 2 presents analysis of the analytical
113 relationship between N , $N\bar{D}$, β , q , D_v and mixing fraction μ for the cases of homogeneous and
114 extreme inhomogeneous mixing. In Sect. 3 the obtained analytical relationships are compared with
115 the results of numerical simulation of N , β , q , D_v formed at the final stage of mixing. Section 4
116 presents results of simulation of progressive mixing and it effect of the relationships between
117 moments. Examples of relationship between N , β , q and D_v from in-situ observations are
118 presented in Sect. 5. The discussion and concluding remarks are presented in Sect. 6 and 7.

119

120 **2 Effect of mixing on microphysical variables**

121 **2.1 Phenomenological consideration**

122 The conceptual diagrams of homogeneous and extreme inhomogeneous mixing are shown on
123 Fig. 1. During the first stage of extreme inhomogeneous mixing the subsaturated parcel is engulfed
124 into the cloudy environment (Fig. 1a1). Then, the droplets at the interface of the sub-saturated

125 parcel and the cloud environment undergo complete evaporation until the air within the engulfed
126 volume reaches saturation (Fig. 1a2). After that the saturated but droplet free parcel mixes with the
127 rest of the cloud environment (Fig. 1a3). The result of inhomogeneous mixing is that the cloud
128 parcel has reduced droplet concentration and the droplet sizes remain unchanged.

129 In the case of homogeneous mixing after entraining into a cloud (Fig. 1b1), the subsaturated
130 parcel “instantly” mixes up with its cloud environment (Fig. 1b2) leading to undersaturation of the
131 total volume. Then, all droplets throughout the mixed volume undergo simultaneous evaporation
132 until the equilibrium state is reached. The result of homogeneous mixing is a cloud volume with
133 reduced concentration of droplets and droplets with reduced sizes (Fig. 1b3).

134 Based on mass and energy conservation the final state of the bulk parameters (i.e. liquid water
135 mixing fraction, humidity, temperature, etc.) is the same for both types of mixing. However, in the
136 case of extreme inhomogeneous mixing saturation is reached through complete evaporation of
137 some fraction of droplets, and their sizes remain constant. Whereas in case of homogeneous mixing
138 saturation is reached through a uniform evaporation of droplets, and the total number of droplets
139 remains unchanged. It should be noted, that in both cases the droplet concentration decreases due
140 to dilution by the mixed droplet free sub-saturated parcel.

141 The following discussion will be specifically focused on the microphysical properties formed
142 at the final stage of the homogeneous and extreme inhomogeneous mixing. The processes
143 occurring during mixing state (i.e. transition 1a→2a and 1b→2b in Fig. 1) remain outside the
144 frame of this work. Following the formalism of homogeneous and extreme inhomogeneous mixing,
145 the process of mixing reaches the final stage when (1) the entrained and cloud environment are
146 mixed up and the spatial gradients of the microphysical (N , β , q , etc.) and environmental (T , S , e ,
147 etc.) parameters approach to zero; (2) the diffusional process related to droplet evaporation comes
148 into equilibrium. The second condition is completed when (a) the environment reaches saturation
149 state, or (b) the entire population of droplets is completely evaporated, if the entrained air is
150 sufficiently dry.

151 The above description of homogeneous and extreme inhomogeneous mixing is highly
152 idealized. Actual in-cloud mixing does not occur as a sequence of discrete events (Fig.1) that
153 individually come to equilibrium only to be followed by next discrete mixing events. But rather it
154 is occurring continuously on a cascade of different spatial and time scales. Broadwell and
155 Breidenthal (1982) summarized the experimental evidence and proposed the following description

156 of mixing in turbulent shear layers. Mixing takes place in a series of events. Two shear layers
157 exchange mass by engulfing parcels from an opposite layer into localized zones. The initially
158 large-scale filaments of the two gases break down towards smaller scales due to the action of
159 turbulence. The turbulence stretches the interface between the gases and enhances the molecular
160 diffusion across the increasing surface. The actual mixing of the engulfed volume is a molecular
161 diffusion process that is most effective after the break down volumes reduce to the Kolmogorov
162 viscosity scale. It is anticipated that the reaction of the ensemble of droplets is a combination of
163 homogeneous and inhomogeneous mixing with domination of one type of mixing over the other
164 depending on the characteristic spatial and time scales of the environment determined by
165 turbulence, cloud microphysics, state parameters and stage of mixing.

166

167 **2.2 Methodology**

168 The foregoing discussion will be focused on mixing between saturated cloud parcels and out-
169 of-cloud sub-saturated air. The cloud parcel contains droplets with average diameter \bar{D}_1 , liquid
170 mixing ratio q_1 and number concentration N_1 . The initial temperature in the cloud parcel is T_1 ,
171 relative humidity $RH_1 = 1$, where $RH = e/e_s(T)$ (the explanation of variable notations is provided
172 in Table 1). The second parcel is droplet free ($N_2 = 0$), sub-saturated with initial relative humidity
173 $RH_2 < 1$ and temperature T_2 . The mixing occurs isobarically, i.e. $p = \text{const}$. At the final stage of
174 mixing the temperature and humidity formed in the resulting parcel are T and RH (appendix A).
175 The process of mixing is completed when the mixed parcel reaches equilibrium due to the air
176 saturation (i.e. $RH = 1$.) or due to the complete evaporation of droplets. In the latter case the final
177 humidity is $RH \leq 1$. The effect of the vertical velocity and vertical travel on final T , RH , and q is
178 not considered here, i.e. vertical velocity $u_z = 0$.

179 Without the loss of generality the masses of the cloudy and sub-saturated volumes prior to the
180 mixing are assumed to have a unit masses, i.e. $m_1 = 1$ and $m_2 = 1$. The mixing process will be
181 considered as mixing of μ fraction of the cloud parcel with $(1 - \mu)$ fraction of the second (sub-
182 saturated) parcel. The mixing cloud fraction may vary within the range of $0 \leq \mu \leq 1$. Therefore,
183 the mass of the resulting mixed parcel is equal to $m_1\mu + (1 - \mu)m_2 = 1$. This approach
184 simplifies the consideration of mixing and allows considering all possible proportions of the
185 mixing of two volumes.

186

2.3 Effect of mixing on liquid water and temperature

The mixing ratio of liquid water q formed at the final stage of mixing is determined by the mass of the mixing cloud water μq_1 and amount of evaporated water required to saturate the newly formed mixed volume δq_m . The mass balance of liquid water for the mixing volume yields

$$q = \mu q_1 - \delta q_m \quad , \quad (1)$$

where

$$\delta q_m = \frac{c_p R_v T_{m0}^2}{L^2} \ln \left(\frac{1 + \frac{e_s(T_{m0}) R_a L^2}{p c_{pa} R_v^2 T_{m0}^2}}{1 + RH_{m0} \frac{e_s(T_{m0}) R_a L^2}{p c_{pa} R_v^2 T_{m0}^2}} \right) \cong - \frac{S_{m0}}{A_2} \quad (2)$$

is the mixing ratio of liquid water required to saturate 1kg of volume with temperature T_{m0} and humidity RH_{m0} (appendix A); T_{m0} , RH_{m0} and S_{m0} , are the temperature, relative humidity formed and supersaturation formed in the volume after instantaneous air mixing, but before droplets start evaporating (appendix A); $e_s(T_{m0})$ is saturation vapor pressure at temperature T_{m0} .

Eq. (1) is a non-linear function of μ , since T_{m0} , e_{m0} and thus δq_m depend on μ . Eq.(1) can be simplified, if $T_1 = T_2$. In this case $T_{m0} = T_1 = T_2$, and $e_s(T_{m0}) = e_s(T_1) = e_s(T_2)$. Given that, the expression under logarithm in Eq.(2) can be expanded in series resulting in (appendix B)

$$\delta q_m = (1 - \mu) \delta q^* \quad , \quad (3)$$

where

$$\delta q^* = \frac{c_p R_v T_2^2}{L^2} \ln \left(\frac{1 + \frac{e_s(T_2) R_a L^2}{p c_{pa} R_v^2 T_2^2}}{1 + RH_2 \frac{e_s(T_2) R_a L^2}{p c_{pa} R_v^2 T_2^2}} \right) \cong - \frac{S_2}{A_2} \quad (4)$$

is the mixing ratio of liquid water required to saturate 1 kg of the entrained dry air. Substituting Eq.(3) in Eq.(1) gives

$$q = \mu q_1 - (1 - \mu) \delta q^* \quad , \quad (5)$$

The value of δq^* does not depend on μ , and Eq. (5) is a simple linear function of μ . The comparisons with numerical simulations showed, that Eq.(5) provides accuracy within few percent, when the temperature difference $|T_1 - T_2| < 2^\circ\text{C}$. Although, in many cases $|T_1 - T_2|$ may vary a

210 wide range reaching 10°C or higher, clouds with $|T_1 - T_2| < 2^\circ\text{C}$ are quite common. Therefore, for
 211 the sake of simplicity, Eq.(5) and the assumption $T_1 \approx T_2$ will be used in the following
 212 consideration of mixing.

213 It should be noted that, Eqs (1) and (5) are valid for the cases, when $\mu > \mu_{cr}$. Here μ_{cr} is
 214 critical mixing fraction, which separates partial and complete evaporation of cloud water in the
 215 mixing volume (section 2.4). Cases when $\mu \leq \mu_{cr}$ correspond to complete evaporation of droplets,
 216 and $q = 0$.

217 The temperature at the final stage of mixing can be estimated as (appendix C)

$$218 \quad T = T_{m0} - \frac{(1 - \mu)\delta q^* L}{c_{pa}}, \quad \text{when } \mu > \mu_{cr} \quad (6a)$$

$$219 \quad T = T_{m0} - \frac{\mu q_1 L}{c_{pa}} \quad \text{when } \mu \leq \mu_{cr} \quad (6b)$$

220 Eqs. (1), (5), (6) were obtained based on mass and energy conservation, and they do not
 221 depend on how mixing proceeds. Therefore, Eqs. (1), (5), (6) are valid for both homogeneous and
 222 inhomogeneous mixing.

223

224 **2.4 Complete evaporation**

225 As mentioned in section 2.2 the process of mixing is complete only after reaching equilibrium
 226 by saturating the mixed volume or by evaporating of all cloud droplets depending on the mixing
 227 fraction μ . The critical mixing fraction μ_{cr} , corresponding to evaporation of all droplets, can be
 228 found from Eq.(5) when $q = 0$, i.e.

$$229 \quad \mu_{cr} = \frac{\delta q^*}{q_1 + \delta q^*} \quad (7)$$

230 Critical mixing fraction separates μ in two subranges: (a) $1 \geq \mu > \mu_{cr}$ where q is described by
 231 Eqs.(1) or (5) and $RH_m = 1$; (b) $\mu_{cr} \geq \mu \geq 0$ where $q = 0$ and $RH_m \leq 1$.

232 For the general case when $T_1 \neq T_2$, μ_{cr} , can be found by solving the non-linear equation

$$233 \quad \mu_{cr} q_1 - \delta q_m(\mu_{cr}) = 0 \quad (8)$$

234 Figure 2 shows comparisons of dependences of μ_{cr} vs. q_1 calculated from Eq. (7) and those
 235 deduced from a numerical model (Sect. 3). Critical mixing fraction μ_{cr} is also shown by black stars
 236 in Fig. 4. The locations of the stars in Fig.4 coincide well with the locations, where the modeled

237 microphysical moments become zero. The obtained agreement between analytical and modeled μ_{cr}
 238 in Figs. 2 and 4 validates the developed approach.

239

240 **2.5 Extreme inhomogeneous mixing**

241 Within the framework of extreme inhomogeneous mixing some fraction of droplets undergo
 242 complete evaporation, whereas the rest of the droplets remain unchanged. Therefore, such a
 243 process results in scaling the droplet size distribution $f(D)$, i.e.

$$244 \quad f(D) = kf_1(D) \quad (9)$$

245 where k is some coefficient dependent on μ and the initial environmental parameters of the mixing
 246 volumes, $f_1(D)$ is the droplet size distribution before mixing. Equation (9) yields relationships
 247 between pairs n th and k -th moments

$$248 \quad \frac{M_n}{M_{n1}} = \frac{M_k}{M_{k1}} \quad (10)$$

249 where $M_n = \int_0^{\infty} f(D)D^n dD / \int_0^{\infty} f(D)dD$ is the n th moment of $f(D)$. Therefore, it is anticipated that
 250 for extreme inhomogeneous mixing droplet number concentration N (0th moment), extinction
 251 coefficient β (2nd moment), liquid water mixing ratio q (3rd moment), along with other moments,
 252 will correlate with each other, i.e.

$$253 \quad \frac{N}{N_1} = \frac{\beta}{\beta_1} = \frac{q}{q_1} \quad (11)$$

254 One of the consequences of Eqs. (9)-(11) is that the characteristic droplet sizes \bar{D} , D_2 , D_v , D_{eff}
 255 will remain constant during inhomogeneous mixing.

256 For the case $T_1 = T_2$ and $\mu > \mu_{cr}$ Eqs. (5) and (11) yield the dependence of N vs. μ

$$257 \quad N = N_1 \left(\mu - \frac{(1-\mu)\delta q^*}{q_1} \right) \quad (12)$$

$$258 \quad \beta = \beta_1 \left(\mu - \frac{(1-\mu)\delta q^*}{q_1} \right) \quad (13)$$

259 For a general case when $T_1 \neq T_2$ the term $(1-\mu)\delta q^*$ in Eqs. (12) and (13) should be replaced
 260 by $\delta q_m(\mu)$ (Eq.(2)).

261

262 **2.6 Homogeneous mixing**

263 For homogeneous mixing, when $\mu > \mu_{cr}$, the droplet number concentration changes only due
 264 to dilution by the entrained air, i.e.

$$265 \quad \frac{N}{N_1} = \mu \quad (14)$$

266 Assuming $T_1 = T_2$, and substituting Eq. (5) in (14) yields:

$$267 \quad \frac{N}{N_1} = \frac{q + \delta q^*}{q_1 + \delta q^*} \quad (15)$$

268 As follows from Eq. (15) N and q are linearly related for homogeneous mixing. However, no
 269 linear relationships exist between other moments. Thus, substituting the definition of the liquid
 270 water mixing ratio $q = \pi \rho_w N D_v^3 / 6 \rho_a$ in Eq. (15) yields the relationship between mean volume
 271 droplet size and concentration

$$272 \quad \frac{D_v^3}{D_{v1}^3} = 1 + \left(1 - \frac{N_0}{N}\right) \frac{\delta q^*}{q_1} \quad (16a)$$

$$273 \quad \frac{D_v^3}{D_{v1}^3} = \frac{q}{q_1} \left(\frac{q_1 + \delta q^*}{q + \delta q^*} \right) \quad (16b)$$

274 In a similar way the relationship between the extinction coefficient $\beta = Q \pi N D_2^2 / 4$, N and q
 275 can be written as

$$276 \quad \frac{\beta}{\beta_1} = \frac{N}{N_1} \left(1 + \left(1 - \frac{N_0}{N}\right) \frac{\delta q^*}{q_1} \right)^{2/3} \quad (17a)$$

$$277 \quad \frac{\beta}{\beta_1} = \left(\frac{q}{q_1} \right)^{2/3} \left(\frac{q + \delta q^*}{q_1 + \delta q^*} \right)^{1/3} \quad (17b)$$

278 In Eqs. (17a) and (17b) it is assumed that $D_2 \approx D_v$.

279 Substituting in Eq. (16) the expression for the time of phase relaxation
 280 $\tau_p = 1/bN\bar{D}$ (e.g. Squires 1953; Korolev and Mazin, 2003) and assuming $\bar{D} \approx D_v$ yields

$$281 \quad \frac{\tau}{\tau_1} = \frac{N_1}{N} \left(1 + \left(1 - \frac{N_1}{N}\right) \frac{\delta q^*}{q_1} \right)^{-1/3} \quad (18)$$

282 For the cases when the temperature difference $|T_1 - T_2|$ exceeds a few degrees, the effect of μ
 283 on T_m and S_m should be taken into consideration in the calculations of evaporated water. For such

284 cases δq_m (Eq. (2)) should be used instead of δq^* . Using Eq. (14) δq_m can be presented as a
 285 function of $\frac{N}{N_1}$, i.e. $\delta q_m(\mu) = \delta q_m\left(\frac{N}{N_1}\right)$. Replacing Eq. (5) by (1) in the above consideration, the
 286 equations Eqs. (15)-(18) can be rewritten as

$$287 \quad \frac{N}{N_1} = \frac{q + \delta q_m\left(\frac{N}{N_1}\right)}{q_1} \quad (19)$$

$$288 \quad \frac{D_v^3}{D_{v1}^3} = 1 - \frac{\delta q_m\left(\frac{N}{N_1}\right) N_1}{q_1 N} = \frac{q}{q + \delta q_m\left(\frac{q}{q_1}\right)} \quad (20)$$

$$289 \quad \frac{\beta}{\beta_1} = \frac{N}{N_1} \left(1 - \frac{\delta q_m\left(\frac{N}{N_1}\right) N}{q_1 N_1} \right)^{2/3} = \frac{q^{2/3} \left(q + \delta q_m\left(\frac{\beta}{\beta_1}\right) \right)^{1/3}}{q_1} \quad (21)$$

$$290 \quad \frac{\tau_p}{\tau_{p1}} = \frac{N_1}{N} \left(1 - \frac{\delta q_m\left(\frac{N}{N_0}\right) N_1}{q_1 N} \right)^{-1/3} \quad (22)$$

291 Eqs. (19)–(22) can be solved numerically.

292

293 **2.7 Degenerate case**

294 As follows from Eq.(5), if

$$295 \quad \frac{(1-\mu) \delta q^*}{\mu q_1} \ll 1 \quad (23)$$

296 then $q_1 \geq q \gg \delta q^*$. If the condition in Eq. (23) is valid, then the terms associated with δq^* in Eqs.
 297 (15)-(18) can be neglected. This results in correlation of all moments, i.e. $N/N_1 = \beta/\beta_1 = q/q_1$
 298 (compare with Eq.(11)). This corresponds to the degenerate case, when the difference between the
 299 homogeneous and inhomogeneous mixing vanishes. Thus, the dimensionless parameter $\xi =$

300 $\frac{1-\mu}{\mu} \frac{\delta q^*}{q_1}$ can be used for characterization of proximity of the homogeneous mixing moments to those

301 formed during extremely inhomogeneous mixing.

302 The range of μ in ξ is limited by $\mu_{cr} < \mu \leq 1$, so that $0 < \frac{1-\mu}{\mu} \leq \frac{q_1}{\delta q^*}$. This gives the range of
 303 changes of ξ , i.e. $0 \leq \xi \leq 1$ for the mixing without complete evaporation of droplets. The
 304 degenerate case corresponds to $\xi \rightarrow 0$, whereas $\xi \rightarrow 1$ corresponds to maximum difference of the
 305 moments for homogeneous and extremely inhomogeneous mixing.

306 As follows from Eqs. (4) and (23) approaching to the degenerate case ($\xi \rightarrow 0$) occurs, when
 307 one of the following conditions or their combination is satisfied: (a) $RH_2 \rightarrow 1$; (b) $E_s(T) \rightarrow 0$ at
 308 low temperatures; (c) $q_1 \gg \delta q^*$; (d) $\mu \rightarrow 1$. The effect of RH , T , q_1 and μ on mixing will be
 309 demonstrated in Sect.3.

310 Figure 3 shows dependence of ξ vs. μ . The grey area in Fig.3 indicates the region where
 311 identification of type of mixing from in-situ measurements (Sect.5) may be hindered due to
 312 proximity of the moments for homogeneous and inhomogeneous mixing. Thus for $\delta q^*/q_1 = 0.01$
 313 identification of type of mixing is ambiguous for nearly the entire range of μ .

314 For the general case, when $T_1 \neq T_2$, it should be $\xi = \frac{|\delta q_m(\mu)|}{\mu q_1}$. An absolute value $|\delta q_m(\mu)|$
 315 should be used in ξ since $\delta q_m(\mu)$ can be negative (Appendix A, Fig.A1) if mixing results in
 316 supersaturation Sect. 3.4).

317 The coefficient ξ may be useful for identification type of mixing from in-situ observations. It
 318 is worth nothing, that the ratio $\frac{\delta q^*}{q_1} \cong \frac{S_2}{A_2 q_1}$ is equal to the parameter R (Pinsky et al. 2015ab), which
 319 plays an important role in determining scenarios of droplet evaporation in turbulent environment.

320

321 **3 Comparisons with numerical simulations**

322 Numerical simulations were performed to examine accuracy and limitations of the analytical
 323 expressions in Sect.2 and to conduct a sensitivity test to environmental and cloud parameters. The
 324 simulations have been performed with the help of a parcel model similar to that in Korolev (1995).
 325 The ensemble of droplets in the simulation was assumed to be monodisperse. For the case of
 326 extreme inhomogeneous mixing the amount of evaporated water Δq required to saturate the mixed
 327 volume was calculated first. If $\Delta q < \mu q_1$, then the concentration of evaporated droplets was
 328 calculated as $N_{ev} = \frac{\Delta q}{m_d} \rho_a$, where $m_d = \pi \rho_w D^3 / 6$. Then, the concentration of the remaining
 329 droplets $N = N_1 - N_{ev}$ was recalculated based of the calculation on the volume formed after
 330 mixing. If $\Delta q \geq \mu q_1$, then all droplets evaporate, and $N = 0$.

331 For the case of homogeneous mixing in the first step the engulfed parcel instantly mixes with
332 the cloud parcel resulting in a new humidity RH_{m0} , temperature T_{m0} and volume V_{m0} . After that
333 the droplets start evaporating until either their complete evaporation or saturation over liquid is
334 reached. The calculations stopped when, either $D < 0.2\mu\text{m}$ or $(E_S - e)/E_S < 0.001$, respectively.

335

336 **3.1 Effect of mixing fraction**

337 Figure 4 shows the results of the simulation of different moments and state parameters vs. μ .
338 The calculations were performed for different relative humidity of the entrained parcel $RH_2 = 0.2,$
339 $0.5, 0.8$ and 0.95 . As seen from Fig.4 for the case of homogeneous mixing only N and q are
340 linearly related with μ , the rest of the variables have non-linear dependences on μ . For the case of
341 inhomogeneous mixing all $f(D)$ moments and droplet sizes linearly depend on μ . Note, for $\mu \leq$
342 μ_{cr} all moments are equal to zero.

343 Since the amount of the evaporated liquid water does not depend on the type of mixing, the
344 dependences of $q(\mu)$ are the same for both homogeneous and inhomogeneous mixing (Fig.4a). The
345 type of mixing has the most pronounced effect on the droplet concentration (Fig.4b) and droplet
346 sizes (Fig.4e).

347 Figure 4g shows the dependences RH_{m0} and RH vs. μ , Here RH_{m0} is the relative humidity at
348 the initial stage of homogeneous mixing before droplets start evaporating (Fig. 1b2). Figure 3h
349 presents comparisons of modeled $T(\mu)$ and those calculated from Eqs.(6a,b) and (C4). The
350 independence of $q(\mu)$, $RH(\mu)$ and $T(\mu)$ on type of mixing (Fig.4a,g,h) is the consequence of the
351 mass and energy conservation, which are not contingent on type of mixing.

352

353 **3.2 Effect of humidity of entrained air**

354 The diagrams in Fig. 5a-c show the dependences of normalized β , q and D_v vs. N/N_0
355 calculated from numerical simulations and analytical equations from Sect. 2. The calculations were
356 performed for different humidity of the entrained air RH_2 . As seen from Fig. 5a-c, the normalized
357 dependences for homogeneous mixing $q(N)$, $\beta(N)$ and $D_v(N)$ tend to approach the line of extreme
358 inhomogeneous mixing when relative humidity RH_2 approaches to 1. This is consistent with the
359 degenerate case, when $\xi \rightarrow 0$ (Sect.2.7). In this case droplets behave as a passive admixture, and
360 they do not interact with the environment.

361

3.3 Effect of liquid water mixing ratio

Figure 5d-f demonstrate the sensitivity of $q(N)$, $\beta(N)$ and $D_v(N)$ to liquid water mixing ratio q_1 . It is seen, that the increase of q_1 results in $q(N)$, $\beta(N)$ and $D_v(N)$ (calculated for homogeneous mixing) approaching towards $q(N)$, $\beta(N)$ and $D_v(N)$ for the inhomogeneous mixing. In other words, the sensitivity of the microphysical parameters to the type of mixing increases with the decrease of q_1 . From a practical viewpoint it means, that from in-situ observations the difference between homogeneous and inhomogeneous mixing is anticipated to be more pronounced for the cases with a relatively low liquid water mixing ratio (e.g. $q_1 < 1\text{g/kg}$). Such behaviour is consistent with the consideration in Sect. 2.7.

3.4 Effect of temperature $T_1 = T_2$

Figure 5g-j shows the effect of temperature on the normalized $q(N)$, $\beta(N)$ and $D_v(N)$ for $T_1 = T_2$. Figure 5g-j indicate that the difference between the moments becomes most pronounced at warm temperatures, whereas at cold temperatures (e.g. $T = -30^\circ\text{C}$), $q(N)$, $\beta(N)$ and $D_v(N)$ for homogeneous mixing are approaching those for the extreme inhomogeneous mixing limit.

Such behavior is explained by the fact that liquid water deficit δq_m decreases with decreasing temperature (appendix A, Fig. A1). At low temperatures ($T = -30^\circ\text{C}$) the amount of evaporated water δq_m is so small, that homogeneous mixing with dry out-of-cloud air will have approximately the same effect as mixing with saturated air (i.e. degenerate case, Sect. 2.7).

Overall, as follows from Fig.5 the results the analytical predictions (Sect. 2) turned out to be in a good agreement with numerical simulations.

3.5 Effect of temperature $T_1 \neq T_2$

Isobaric mixing of two nearly saturated volumes with $T_1 \neq T_2$ may result in supersaturated environment (e.g. Rogers, 1976; Bohren and Albrecht, 1998). Mixing resulting in supersaturation is different in principle from the mixing with evaporating droplets. In this case the meaning of homogeneous and inhomogeneous mixing becomes ambiguous. Formation of supersaturation leads to different dependences between $N\bar{D}$, β , q , \bar{D} and N as compared to those shown in Figs. 3–4, when $T_1 = T_2$.

Figure 6 presents a set of diagrams similar to those in Fig.4, but calculated for the cases when $T_1 \leq T_2$. It turns out that for the case of extreme inhomogeneous mixing the temperature difference

393 between T_1 and T_2 breaks down linear dependences of the microphysical moments (e.g. $N\bar{D}$, β , q
394 Fig. 6a,c,d) vs. μ .

395 Figure 7 presents the effect of the temperature difference ΔT on the normalized dependences
396 $q(N)$, $\beta(N)$ and $D_v(N)$. In clouds, high supersaturation resulting from isobaric mixing may lead to
397 activation of interstitial CCN, which may increase N and decrease D_v (Korolev and Isaac, 2000).
398 However, no activation of new droplets during isobaric mixing was allowed in this study. For the
399 cases when $RH_{m0} > 1$ (Fig. 7, AB on line 1) the condensed water was uniformly distributed
400 between available droplets. Therefore, $q(N)$, $\beta(N)$ and $D_v(N)$ calculated for homogeneous and
401 extremely inhomogeneous mixing coincide with each other on this interval.

402 Numerical simulations also showed, that the effect of temperature on mixing is more
403 pronounced for the cases when the cloud temperature is warmer than that of the entrained air, i.e.
404 $T_1 > T_2$, as compared to the cases with $T_1 < T_2$.

405

406 **4. Progressive mixing**

407 **4.1 Effect on microphysical parameters**

408 In the previous sections the mixing was considered as a single event, i.e. μ fraction of the
409 cloudy air mixed up with $(1 - \mu)$ fraction of entrained dry air. Such mixing will be referred to as
410 “primary” mixing. Primary mixing results in an ensemble of elementary volumes characterized by
411 a set of microphysical and state parameters i.e. $\bar{D}(\mu)$, $N(\mu)$, $RH(\mu)$, $T(\mu)$, etc. Each of these
412 parameters has a functional dependence on μ , and what is important, these parameters have
413 functional relationships between each other.

414 In reality mixing is a continuous process. It does not stop after the primary mixing. The
415 elementary volumes formed after primary mixing continue to progressively mix with each other.

416 The second stage of mixing will result in an ensemble of elementary volumes characterized by
417 a set of parameters $D_v^{(2)}$, $N^{(2)}$, $RH^{(2)}$, $T^{(2)}$, etc. Here the superscript ⁽²⁾ indicates the stage of
418 mixing. After the second stage the mixed volumes undergo subsequent stages of mixing.

419 The idealised conceptual diagram of the progressive mixing is shown in Fig. 8. As mentioned
420 in Sect. 2.1, the actual process of mixing is indeed much more complex than the sequence of
421 discrete events portrayed in Fig.8. However, as it will be shown below, this simplified
422 consideration of allows establishing main features of evolution of relationships between the

423 microphysical moments affected by mixing. The obtained results facilitates identification of type of
424 mixing from in-situ measurements.

425 Progressive mixing was simulated with the help of a numerical model, where parcels were
426 randomly mixed with each other and with the cloud environment. The mixing fraction μ was also
427 set to be random during each mixing event. Models of stochastic mixing have been used in a
428 number of studies (e.g. Krueger et al., 1997; Su et al., 1998; Burnet and Brenguier, 2007). In the
429 present work the analysis of progressive mixing is expanded to examine its effect on the
430 relationship between moments of the droplet size distribution.

431 The results of the progressive mixing for the first four stages are presented in Fig. 9. As seen
432 from Fig. 9 the functional relationship between the pairs of microphysical and state parameters
433 exists only for the primary stage. For higher mixing stages these functional relationships break
434 down. Thus, cloud volumes with the same $N^{(2)}$ may have different $D_v^{(2)}$. Figure 9 also shows that
435 the regions of scattering of $q(N)$, $\beta(N)$ and $D_v(N)$ for stages 2, 3 and 4 are limited from above by
436 the inhomogeneous mixing (red dashed lines) and from below by primary homogeneous mixing
437 (red solid lines).

438 Figure 10 presents a conceptual $N - q$ diagram explaining breaking the functional
439 relationships during progressive homogeneous mixing. After the first stage of mixing the $N - q$
440 points will be scattered along the line OB and point C . The line OB corresponds to the ensemble of
441 points with $RH = 1$. Therefore, result of mixing between two saturated volumes randomly selected
442 on AB , will remain on the same line. Point C corresponds to the ensemble of points with $N = 0$,
443 $RH_2 \leq RH_C(\mu^{(1)}) \leq 1$, where $0 \leq \mu^{(1)} < \mu_{cr}$. Therefore, mixing between point A (Fig.10) and
444 point C , when $RH = 1$ will result in scattering along the line AC (degenerate case). Points resulted
445 from mixing between A ($RH = 1$) and point C , when $RH_2 \leq RH_C < 1$, will scattered over the
446 ensemble of dashed lines shown in Fig.10. These lines will fill the sector CAB . Random mixing
447 between points on the line OB and C , will eventually fill the entire sector COB . The same
448 consideration can be applied to progressive mixing between other moments.

449 During the progressive mixing $N^{(n)}$, $\beta^{(n)}$, $q^{(n)}$ and $D_v^{(n)}$ formed in the elementary parcels tend
450 to approach those in the undiluted cloud, i.e. N_1 , β_1 , q_1 and D_{v1} . This process can be considered as
451 a surrogate to the diffusion process between the cloud and sub-saturated out-of-cloud environment.
452 The convergence of $\beta^{(n)}$, $q^{(n)}$ and $D_v^{(n)}$ during the progressive mixing can be seen in Fig. 9, where

453 the scattering of normalized $q^{(n)}(N)$, $\beta^{(n)}(N)$ and $D_v^{(n)}(N)$ becomes denser towards the top-right
454 corner (1,1) with the increase of the stage of mixing.

455 It is worth noting that progressive mixing with the dry air does not break the functional
456 relationships between the moments. This case is equivalent to detrainment of cloudy environment
457 into dry air. It can be shown that Eq.(14) remain valid at any stage of progressive homogeneous
458 mixing with dry air only, i.e. $N_j/N_1 = \mu^{(1)} \dots \mu^{(j-1)} \mu^{(j)}$ where $\mu^{(j)}$ is the mixing fraction at the j -
459 th stage of mixing. Eqs. (15)-(24) also remain valid for the progressive mixing with the dry air
460 only.

461 As follows from Eq. (9) for the case of extreme inhomogeneous mixing the progressive mixing
462 does not affect the functional relations between $N^{(n)}$, $\beta^{(n)}$, $q^{(n)}$ and $D_v^{(n)}$ and other microphysical
463 parameters. These relations remain the same regardless of the actual stage of mixing. This is one of
464 the fundamental differences between homogeneous and inhomogeneous mixing, which can be used
465 for identification of type of mixing from in-situ measurements.

466

467 **4.2 Effect on droplet size distributions**

468 Figure 11 shows modeled droplet size distributions averaged over the ensembles of elementary
469 volumes corresponding to the first four stages of homogeneous mixing. As seen from Fig. 11a–d
470 for the case with $T_1 = T_2$ the droplet size distributions are broadened towards small sizes.
471 Depending on the stage of mixing and mixing fraction μ the size distributions formed in each
472 elementary volume may be unimodal or multimodal. However, due to the random nature of the
473 modal sizes formed during mixing, the average size distributions become smooth and unimodal
474 (Fig.11a-d).

475 Broadening of droplet size distributions towards small sizes during homogeneous mixing is
476 well known and it was demonstrated in a number of studies (e.g. Baker and Latham, 1982; Jensen
477 and Baker, 1989; Jeffery, 2007; Kumar et al., 2013). However, if mixing results in supersaturation
478 (section 3.4), then the droplet size distribution may broaden towards larger sizes (Fig. 11e–h). For
479 this to occur, both the temperature difference between the cloud and the environment $|T_1 - T_2|$ and
480 the relative humidity of the environment RH_2 must be sufficiently large. Such conditions are
481 inherently unstable, however, this might occur in regions that have been moistened through prior
482 cloud detrainment. Thus homogeneous mixing may result in broadening of droplet size
483 distributions towards either smaller or larger sizes (Fig.11).

484 These results were obtained in the frame of the formalism of homogeneous and
485 inhomogeneous mixing. The following two works in this series (Pinsky et al., 2015a, b) will
486 discuss the broadening of polydisperse and monodisperse $f(D)$ during both homogeneous and
487 inhomogeneous mixing in greater details.

488

489 **5 Identification of type of mixing from in-situ observations**

490 The purpose of this section is to attempt identifying type of mixing based on examining
491 relationships between basic microphysical parameters N , β , LWC , D_v measured from in-situ.

492 **5.1 Expected relationships between the moments**

493 Prior proceeding with the analysis of in-situ data we summarize the results of the previous
494 consideration on how homogeneous and extreme inhomogeneous mixing is expected to manifest
495 itself in relationships between basic microphysical parameters, such as N , β , q and D_v .

496 For extreme inhomogeneous mixing the relationship between the pairs of N , β and q are
497 determined by linear dependences $M_n = \alpha_{nk}M_k$ (Eq. 10) at any stage of mixing. As follows from
498 Eq. (11) the slopes α_{nk} for $q(N)$, $\beta(N)$ and $q(\beta)$ are equal to the ratios q_1/N_1 , β_1/N_1 , and q_1/β_1 ,
499 respectively, where N_1 , β_1 and q_1 correspond to undiluted adiabatic values. The values of N_1 , β_1
500 and q_1 may vary depending on the location inside the cloud and environmental conditions at the
501 cloud base. Thus, the adiabatic value of q_1 is a function of elevation above the cloud base ΔZ ,
502 whereas N_1 depends on the vertical velocity at the cloud base u_z and the aerosol load. Therefore,
503 the scattering of $q - N$ points will be aligned along an ensemble of different lines determined by
504 q_1/N_1 , which are specific to different cloud volumes. The conceptual diagram of the scattering of
505 $q - N$ measurements in a cloud with extreme inhomogeneous mixing is shown in Fig. 12a. The
506 scatter diagrams for other moments (e.g. $q - \beta$, $N - \beta$) will have the similar patterns as that in Fig.
507 12a.

508 For the case of homogeneous mixing the functional relationship between the pairs of N , β , q
509 and D_v are disrupted by a progressive mixing. As shown in Sect. 4.1 the ensemble of points of N , β
510 and q will be scattered within a sector, which is limited by lines determined by Eq. (11) (extreme
511 inhomogeneous mixing) and Eqs. (15)-(17) (primary homogeneous), respectively (Fig. 9). What is
512 important, is that the top of the sectors for $q(N)$ and $\beta(N)$ correspond to points $[N_1, q_1]$ and
513 $[N_1, \beta_1]$, respectively. Since N_1 , β_1 and q_1 may vary within the same cloud, it is anticipated that the
514 N , β and q measurements will be scattered within an ensemble of sectors as shown in Fig. 12b.

515 It is important to note that that during homogeneous mixing prior reaching equilibrium,
516 functional relationships between the microphysical moments do not exist either. After the instant
517 mixing of cloud fraction μ with entrained air (Fig. 1b(2)), $q_{m0} = \mu q_0$ and $N_{m0} = \mu N_0$. This state
518 corresponds to point D in Fig.10. After that droplets start evaporating until liquid mixing ratio
519 reaches point A (Fig.10), which corresponds to the equilibrium state ($RH = 1$). Therefore, during
520 evaporation time $q - N$ points will be scattered along the line AD . Since, point D can be located
521 anywhere on OC , the ensemble of $q - N$ points corresponding to non-equilibrium state will fill the
522 COB area.

523 Thus, the absence of the functional relationships between the moments during homogeneous
524 mixing may occur both during progressive mixing and during primary mixing prior reaching the
525 equilibrium state. The evaporation time required to reach equilibrium during homogeneous mixing
526 is discussed in details in Pinsky et al. (2015b), and it is usually limited by few tens of seconds.
527 However, progressive mixing is not limited in time. Therefore, it is very likely that no functional
528 relationship between microphysical parameters will be observed during in-situ measurements.

529 Fig.12 demonstrated a fundamental difference in scattering of $q - N$ for homogeneous and
530 extreme inhomogeneous mixing, which will be used to facilitate identification of type of mixing in
531 the following section.

532

533 **5.2 Results of observations**

534 The measurements were obtained on the University of Wyoming King Air aircraft during the
535 COPE-MED project in South-Western part of UK during July-August 2013 (Leon et al., 2016).
536 The UW King Air was equipped with a suite of microphysical instruments, including a DMT
537 Cloud Droplet probe (CDP), designed for measurements of droplet sizes and their concentrations in
538 the nominal size ranges 1–50 μm .

539 Figure 13 shows a time series of droplet concentration, extinction coefficient, liquid water
540 content and mean volume droplet diameter measured by the CDP during transit through a
541 convective cell on 18 July 2013. The CDP data were sampled at 10Hz, which corresponds to
542 approximately 10m spatial averaging. Visual examination of the spatial changes of N , β and LWC
543 shows strong correlation. The amplitude of changes of these parameters reaches nearly one
544 hundred percent with respect to their maximum. Contrary to that, the spatial variations of \bar{D} and D_v
545 are quite conservative and their values remain nearly constant. With the exception of two cloud

546 holes between 13:50:42 and 13:50:44, the amplitude of fluctuations of D_v does not exceed 8% with
547 standard deviation of 2.2%.

548 Figure 14 shows scatter diagrams of $LWC(N)$, $\beta(N)$, $LWC(\beta)$ and $D_v(N)$ measured by the
549 CDP during seven consecutive penetrations of the same convective cell extended over a period of
550 approximately 19 min. One of these penetrations is shown in Fig. 13. The measurements were
551 conducted at $H = 5500\text{m}$ and $T = -12^\circ\text{C}$. The relative humidity of the ambient air was
552 approximately 20 %. At the beginning of the sampling no precipitation size particles were observed
553 in the cloud. However, by the end of the sampling period some raindrops and ice crystals were
554 present in the cloud. Despite the presence of some precipitation size particles, the scatter diagrams
555 in Fig. 14a, b and d demonstrate high correlation between pairs N , β and LWC . The mean volume
556 diameter in Fig. 14c shows very little changes from 19 to 17 μm when concentration changes from
557 1100 to 500 cm^{-3} , However, for $N < 200 \text{ cm}^{-3}$, the volume diameter decreases to 12–15 μm .

558 Red lines in Fig. 14 indicate $q(N)$, $\beta(N)$, $LWC(\beta)$ and $D_v(N)$ calculated for the 1st stage of
559 homogeneous mixing. The calculations were performed for a monodisperse $f(D)$ with $D_1=18.5\mu\text{m}$,
560 $N_1 = 1100 \text{ cm}^{-3}$, and state parameters as during the measurements. Comparisons of dependences
561 $q(N)$, $\beta(N)$, $LWC(\beta)$ and $D_v(N)$ based on in-situ measurements with those obtained from
562 numerical simulations of homogeneous mixing show minor difference for high concentrations 700
563 $\text{cm}^{-3} < N < 1100 \text{ cm}^{-3}$ (Fig. 14a–c). Simulation also shows that for this specific case the difference
564 between homogeneous and inhomogeneous mixing does not exceed 10% when $700 \text{ cm}^{-3} < N <$
565 1100 cm^{-3} . Such difference remains within the errors of measurements. Therefore, in this specific
566 cloud for the regions with $N > 700 \text{ cm}^{-3}$ the type of mixing cannot be unambiguously identified
567 from the analysis of the dependences $LWC(N)$, $\beta(N)$, $LWC(\beta)$ and $D_v(N)$. This is consistent with
568 the assessment of feasibility of segregation of homogeneous and inhomogeneous mixing in Fig.3
569 (dashed line). Since for homogeneous mixing $N \propto \mu$, than Fig.3 suggests good separation of the
570 moments for $N > 700 \text{ cm}^{-3}$.

571 For the regions with $N < 500 \text{ cm}^{-3}$ the deviation between homogeneous mixing simulations
572 and in-situ measurements in Fig.14 becomes well pronounced and it extends beyond possible errors
573 of measurements. This suggests that the mixing in these regions is dominated by the extreme
574 inhomogeneous type.

575 Figure 15 shows the same type of diagrams as in Fig. 14, which were measured during 45
576 consecutive traverses through an ensemble of deep convective cells. The sampling altitude varied

577 in the range $3000\text{m} < H < 4500\text{m}$, temperature $-11^\circ\text{C} < T < 0^\circ\text{C}$, relative humidity in the vicinity of
578 clouds $15\% < \text{RH} < 65\%$. The cloud measurements were extended over a period of 2 h 13 m, which
579 is suggestive that the convective cells were sampled at different stages of their lifetime. At the
580 sampling level the concentration of raindrops varied from zero to few per liter, and their diameter
581 did not exceed 2mm.

582 What is interesting that the scattering of the measurements $LWC(N)$, $\beta(N)$ and $LWC(\beta)$ (Fig.
583 15a, b and d) is limited by the sector, which originates from the zero point as in Fig.12a. Analysis
584 of the measurements showed that the data points $LWC(N)$, $\beta(N)$, $LWC(\beta)$ in each individual
585 cloud traverse are well aligned along the lines with different slopes (e.g. Fig.14). After averaging
586 over the ensemble of clouds, the area of the scattered points turned out to be located inside a sector
587 limited by the lines with smallest and largest slopes.

588 Comparisons of the scatterdiagrams $LWC(N)$, $\beta(N)$ and $LWC(\beta)$ in Figs.14 and 15 with the
589 conceptual diagrams in Fig.12 unambiguously suggest that interaction between cloud and
590 environment in the studied clouds was dominated by inhomogeneous mixing. It should be
591 emphasized that analysis of a stand alone mixing diagram $N - D_v$ would not allow unambiguously
592 draw such conclusion.

593

594 **6. Discussion**

595 One of the assumptions in most past studies is that for a sequence of the cloud samples
596 collected along the flight path, the adiabatic values of N_1 , q_1 , β_1 , D_1 and environmental parameters
597 e_2 and T_2 remain the same. In fact these parameters may vary both within the same cloud or
598 sequence of samples clouds, and the amplitude of their variations depends on microphysical and
599 thermodynamical properties inside and outside the cloud environment. This variation will result in
600 an ensemble of relationships $M_n = F_{nk}(M_k)$, and enhance scattering of the data points. In such
601 cases identification of the type of mixing based on the $N - D_v$ diagram may result in confusion
602 between homogeneous and inhomogeneous mixing. As demonstrated in Sect. 5, consideration of
603 $N - q$ and $N - \beta$ diagrams may provide a better identification type of mixing.

604 Strictly speaking the identification of type of mixing from particle probe measurements as it
605 was performed in Sect. 5 is incomplete. It allows establishing correlation between microphysical
606 moments and makes a formal conclusion about the mixing type, however it does not allow
607 judgement about stage of mixing (i.e. whether mixing is complete by reaching equilibrium). In

608 most previous studies, including this one, identification of type of mixing was based on the
609 assumption that the sampled cloud volume is in equilibrium state ($RH = 1$), and that it reached the
610 final stage of mixing (Fig.1 a2, a3, b3). It is possible that at the moment of measurement the
611 process of mixing is not complete and the droplet free filaments remained undersaturated (Fig.1 a1,
612 b1, b2). In this case the relationship between different moments may be well described as $M_n =$
613 $\alpha_{nk}M_{nk}$ and the mixing be confused with inhomogeneous mixing.

614 In order to identify stage of mixing, high frequency collocated measurements of temperature
615 and humidity are required. Unfortunately current technology does not allow such measurements
616 yet.

617 Identification of type of mixing from in-situ observations is based on examination of
618 relationships between moments of the size distributions measured along the flight path. The basic
619 assumption underlying this analysis is that the cloud environment is not affected by other non-
620 adiabatic processes.

621 Thus, collision-coalescence, riming or Wegener-Bergeron-Findeisen processes may change the
622 droplet number concentration and liquid water content, and therefore, affect the relationship
623 between the moments. Activation of interstitial CCN will result in breaking correlation between the
624 moments due to formation of large concentration of droplets. Broad size distributions may also
625 hinder identification of type of mixing due to partial evaporation of small droplets (Pinsky et al.
626 2015a)

627 It is anticipated that most suitable candidates to study mixing-entrainment process are non-
628 precipitating convective clouds and stratocumulus clouds with relatively narrow droplet size
629 distributions.

630 Another limiting factor is that the above consideration did not account for the effect of
631 changing relative humidity in a vertically ascending parcel. Thus in droplet free entrained air RH
632 increases approximately 10% for $\Delta z = 200\text{m}$ at $T = 0^\circ\text{C}$. After reaching saturation the mixing
633 turns into a degenerate case, which will appear as extreme inhomogeneous mixing. Joint effects of
634 evaporating droplets and an increase in RH during the vertical ascent may facilitate reaching
635 saturation state. This case may also be relevant to the convective cloud described in Sect.5.2.

636

637

638

639 **7. Conclusions**

640 This study analyzes dependences of different moments of $f(D)$ in the frame of formalism of
641 homogeneous and extremely inhomogeneous mixing. The analysis was performed for the final
642 stage of mixing based on the mass and energy conservation consideration. The following results
643 were obtained in the frame of this study:

644 1. Simple analytical relationships between the main microphysical moments were obtained for
645 the final state homogenous and extreme inhomogeneous mixing.

646 2. It was shown that the functional relationships between the moments exist only for the first
647 stage of homogeneous mixing, when equilibrium is reached. Subsequent progressive homogeneous
648 mixing breaks the functional relationship between the moments.

649 3. It was demonstrated that consideration of scattering $N - LWC$, $N - \beta$ diagrams facilitates
650 identification of type of mixing from in-situ measurements. For extreme inhomogeneous mixing
651 the scattering of the data points $N - LWC$, $N - \beta$ will be limited by a sector originating at zero
652 point (Fig.12a). However, for homogeneous mixing the scattering data points will be limited by a
653 sector originating at (N_1, LWC_1) and (N_1, β_1) (Fig.12b). Utilizing a stand-alone conventional $N -$
654 D_v mixing diagram may not provide unambiguous answer about type of mixing.

655 4. The developed approach was applied to a set of in-situ measurements collected in
656 convective clouds. The analysis of the dependences between N , β , LWC and D_v suggests that the
657 interaction between entrained and cloudy environments for the studied clouds was dominated by
658 inhomogeneous mixing.

659 The present study considers relationships between different moments of $f(D)$ for the final
660 stage of mixing. The following two works Pinsky et al. (2015a, b) in this series provide a detailed
661 analysis of time dependences of droplet size distributions and its moments during homogeneous
662 and inhomogeneous mixing.

663

664 *Acknowledgement.* The authors appreciate two anonymous reviewers for their comments.
665 Alexei Korolev work was supported by Environment Canada and Transport Canada. The COPE-
666 MED project was funded by National Science Foundation grant AGS-1230292 and AGS-1230203.
667 The contribution of Mark Pinsky and Alex Khain was supported by the Israel Science Foundation
668 (grant 1393/14), the Office of Science (BER), US Department of Energy Award DE-SC0006788
669 and the Binational US-Israel Science foundation (grant 2010446).

670

671 **Appendix A: Liquid water deficit**

672 The objective of this section is to find the amount of liquid water, which is required to be
673 evaporated in order to saturate the parcel formed after mixing. Assume that q_{v1} , q_{v2} are the mixing
674 vapor ratios in the cloudy and entrained parcels, respectively, and T_1 , T_2 are their respective initial
675 temperatures. First, we find the saturation ratio S_{m0} formed after instant mixing of the cloud and
676 entrained before the cloud droplets start evaporating.

677 The vapor mixing ratio q_{vm} formed in the mixed volume will be

$$678 \quad q_{vm} = \mu q_{v1} + (1 - \mu) q_{v2} \quad (\text{A1})$$

679 The vapor pressure e_m in the mixed volume can be derived from Eq. (A1) by substituting

$$680 \quad q_v = \frac{e}{p - e} \frac{R_a}{R_v}, \text{ i.e.}$$

$$681 \quad e_m = p \frac{\mu + \frac{e_2(p - e_1)}{p(e_1 - e_2)}}{\mu + \frac{(p - e_1)}{(e_1 - e_2)}} \quad (\text{A2})$$

682 The temperature of the mixed volume T_{m0} can be found from the energy conservation law

$$683 \quad \mu(q_{v1}c_{pv} + c_{pa})(T_1 - T_{m0}) = (1 - \mu)(q_{v2}c_{pv} + c_{pa})(T_{m0} - T_2) \quad (\text{A3})$$

684 here c_{pv} , c_{pa} , are the specific heat capacitance of water vapor and dry air at constant pressure,
685 respectively, T_1 , T_2 are the initial temperatures in the first and second parcels before mixing.
686 Substituting q_{v1} , q_{v2} yields the temperature in the mixed volume

$$687 \quad T_{m0} = \frac{\mu T_1 + \alpha(1 - \mu)T_2}{\mu + \alpha(1 - \mu)} \quad (\text{A4})$$

688 here

$$689 \quad \alpha = \frac{1 + \frac{c_{pv}R_a e_2}{c_{pa}R_v(p - e_2)}}{1 + \frac{c_{pv}R_a e_1}{c_{pa}R_v(p - e_1)}} \quad (\text{A5})$$

690 With a good accuracy $\alpha \cong 1$. The resulting relative humidity after mixing the two volumes
691 will be

692
$$RH_{m0} = \frac{e_{m0}}{e_s(T_{m0})} \quad (\text{A6})$$

693 where $e_s(T_{m0})$ is the saturated vapor pressure at temperature T_{m0} .

694 The process of evaporation is accompanied by changing humidity and temperature due to
 695 latent heat of vaporization. This process is described by the Eq. (C2) in Korolev and Mazin (2003).
 696 Assuming the process to be isobaric (i.e. vertical velocity $u_z = 0$) and absence of ice ($dq_i = 0$),
 697 Eq. (C2) (Korolev and Mazin, 2003) yields

698
$$\frac{dS}{S+1} = \left(\frac{1}{S+1} \frac{pR_v}{e_s R_a} + \frac{L^2}{c_{pa} R_v T^2} \right) dq \quad (\text{A7})$$

699 Integrating Eq. (A7) from initial S_{m0} to saturation state, when $S = 0$, and taking into account
 700 that $RH = S + 1$, gives

701
$$\delta q_m = -b \ln \left(\frac{1 + a RH_{m0}}{1 + a} \right) \quad (\text{A8})$$

702 the mixing ratio of liquid water required to evaporate in order to saturate 1kg of the cloud volume
 703 formed after mixing with the entrained air, but before droplet start evaporating. Here $a = \frac{E_s R_a L^2}{p c_p R_v^2 T_{m0}^2}$,

704
$$b = \frac{c_p R_v T_{m0}^2}{L^2}.$$

705 Since $\left| \frac{A(RH_{m0}-1)}{1+A} \right| < 1$, Eq.(A8) can be simplified as

706
$$\delta q_m = ab \frac{1 - RH_{m0}}{1 + a} = -\frac{S_{m0}}{A_2} \quad (\text{A9})$$

707 where $A_2 = \frac{ab}{1+a}$. The analysis of Eqs. (A8)-(9) shows that for wide range of temperatures $-30 \text{ }^\circ\text{C} <$
 708 $T < 30 \text{ }^\circ\text{C}$, both equations hold with high accuracy as long as the temperatures of the sub-saturated
 709 and cloud parcels $|T_1 - T_2| < 10^\circ\text{C}$.

710 Figure A1 shows comparisons of modeled δq_m and that calculated from Eqs. (A8) and (A9)
 711 for three different temperatures. The model solved a system of differential equation with
 712 incremental evaporation of liquid water until saturation is reached. As seen from Fig. A1 the
 713 agreement between modeled δq_m and that calculated from Eq. (A8)-(A9) is quite good and does
 714 not exceed few percent at $RH_{m0} = 0.5$. This discrepancy results from assumption that e_s and T are
 715 constant in Eqs.(A8)-(A9).

716

717 **Appendix B: Liquid water deficit when $T_1 = T_2$**

718 Eq.(A2) by assuming that $p \gg e_1$ and $p \gg e_2$ can be simplified as

719
$$e_{m0} = \mu e_1 + (1 - \mu)e_2 \quad (\text{B2})$$

720 As follows from Eq.(A4) for the case $T_1 = T_2$ with high accuracy $T_{m0} = T_1 = T_2$. Therefore,
721 $e_s(T_{m0}) = e_s(T_1) = e_s(T_2)$. Dividing Eq.(B1) by e_s yields

722
$$RH_{m0} = \mu RH_1 + (1 - \mu)RH_2 \quad (\text{B3})$$

723 In most liquid clouds $RH_1 = 1$ (Korolev and Mazin 2003). Therefore, Eq.B2 turns into

724
$$RH_{m0} = \mu + (1 - \mu)RH_2 \quad (\text{B4})$$

725 Substituting Eq.(B4) in Eq.(B1) yields

726
$$\delta q_m = -b \ln \left(1 + \frac{a(1 - \mu)(RH_2 - 1)}{1 + a} \right) \quad (\text{B5})$$

727 The expression under logarithm can be presented as the first two terms of the series expansion
728 of $\left(1 + \frac{a(RH_2 - 1)}{1 + a} \right)^{(1 - \mu)}$. Substituting this expression into Eq.(B5), gives

729
$$\delta q_m = (1 - \mu)\delta q^* \quad (\text{B6})$$

730 where

731
$$\delta q^* = -b \ln \left(\frac{1 + aRH_2}{1 + a} \right) \quad (\text{B7})$$

732 is the mixing ratio of liquid water required to saturate 1 kg of the entrained dry volume.

733

734 **Appendix C: Temperature in the mixing volume**

735 The energy conservation for evaporating droplets can be written as

736
$$(T - T_{m0})(1 + q_{vm})c_{pm} + (1 - \mu)\delta q^* L = 0 \quad (\text{C1})$$

737 here c_{pm} is the specific heat capacity of the moist air

738
$$c_{pm} = \frac{c_{pa} + q_{vm}c_{pv}}{1 + q_{vm}} \quad (\text{C2})$$

739 Since $q_{vm} \ll 1$ and, $c_{pa} \cong c_{pm}$ Eq.(C1) may be simplified, so that the final temperature after
740 mixing

741
$$T = T_{m0} - \frac{(1 - \mu)\delta q^* L}{c_{pa}} \quad (\text{C3})$$

742 For the case when $T_1 \neq T_2$ Eq. (C3) should be replaced by

$$743 \quad T = T_{m0} - \frac{\delta q_m L}{c_{pa}} \quad (C4)$$

744 Eqs. (C3) and (C4) are valid for the mixing fraction $\mu > \mu_{cr}$. For $\mu \leq \mu_{cr}$ all entrained liquid
745 water μq_0 evaporates, and the final temperature will be

$$746 \quad T = T_{m0} - \frac{\mu q_0 L}{c_{pa}} \quad (C5)$$

747

748 **References**

- 749 Andrejczuk M., Grabowski, W. W., Malinowski, S. P., and Smolarkiewicz, P. K.: Numerical
750 simulation of cloud–clear air interfacial mixing: homogeneous vs. inhomogeneous mixing., J.
751 Atmos. Sci., 66, 2493-2500, 2009.
- 752 Baker, M. B. and Latham, J.: The evolution of droplet spectra and the rate of production of
753 embryonic raindrops in small cumulus clouds, J. Atmos. Sci., 36, 1612–1615, 1979.
- 754 Baker, M. B. and Latham, J.: A diffusive model of the turbulent mixing of dry and cloudy air, Q. J.
755 R. Met. Soc., 108, 871–898, 1982.
- 756 Baker, M. B., Corbin, R. G., and Latham, J.: The influence of entrainment on the evolution of
757 cloud droplet spectra: I. A model of inhomogeneous mixing, Q. J. Roy. Meteor. Soc., 106, 581–
758 598, 1980.
- 759 Beals, M.J., and Fugal, J.P., Shaw, R.A., Lu, J., Spuler, S.M., Stith, J.L.: Holographic
760 measurements of inhomogeneous cloud mixing at the centimeter scale. Science, 350, 87-90,
761 2015
- 762 Bohren, C. F. and Albrecht, C. H.: Atmospheric Thermodynamics, Oxford University Press, New
763 York, 402 pp., 1998.
- 764 Bower, K. N. and Choulaton, T. W.: The effects of entrainment on the growth of droplets in
765 continental cumulus clouds, Q. J. Roy. Meteor. Soc., 114, 1411–1434, 1988.
- 766 Broadwell, J. E., and R. E. Breidenthal: A simple model of mixing and chemical reaction in a
767 turbulent shear layer. J. Fluid Mech., 125, 397–410, 1982
- 768 Burnet, F. and Brenguier, J. L.: Observational study of the entrainment-mixing process in warm
769 convective clouds, J. Atmos. Sci., 64, 1995–2011, 2007.

770 Devenish, B. J., Bartello, P., Brenguier, J.-L., Collins, L. R., Grabowski, W. W., Ijzermans, R. H.
771 A., Malinowski, S. P., Reeks, M.W., Vassilicos, J. C., Wang, L- P., and Warhaft, Z.: Droplet
772 growth in warm turbulent clouds, *Q. J. Roy. Meteor. Soc.*, 138, 1401–1429, 2012.

773 Dimotakis, P. E.: Turbulent mixing, *Annu. Rev. Fluid Mech.*, 37, 329–356, 2005.

774 Gerber, H., Frick, G., Jensen, J. B., and Hudson, J. G.: Entrainment, mixing, and microphysics in
775 trade-wind cumulus, *J. Meteorol. Soc. Jpn.*, 86, 87–106, 2008.

776 Hill, T. A. and Choulaton, T. W.: An airborne study of the microphysical structure of cumulus
777 clouds, *Q. J. Roy. Meteor. Soc.*, 111, 517–544, 1985.

778 Jeffery, C. A.: Inhomogeneous cloud evaporation, invariance, and Damköhler number, *J. Geoph.*
779 *Res.*, 112, D24S21, doi:10.1029/2007JD008789, 2007.

780 Jarecka, D., Grabowski, W. W., Morrison, H., Pawlowska, H.: Homogeneity of the Subgrid-Scale
781 Turbulent Mixing in Large-Eddy Simulation of Shallow Convection. *J. Atmos. Sci.* 70, 2751-
782 2767, 2013

783 Jensen, J. and Baker, M.: A simple model of droplet spectra evolution during turbulent mixing, *J.*
784 *Atmos. Sci.*, 46, 2812–2829, 1989.

785 Korolev A. V.: The influence of supersaturation fluctuations on droplet spectra formation. *Journal*
786 *of the Atmospheric Sciences*, 52, 3620-3634, 1995.

787 Korolev, A. V. and Isaac, G. A.: Drop growth due to high supersaturation caused by isobaric
788 mixing, *J. Atmos. Sci.*, 57, 1675–1685, 2000.

789 Korolev, A. V. and I.P. Mazin,: Supersaturation of water vapor in clouds. *J. Atmos. Sci.*, 60, 2957-
790 2974, 2003.

791 Krueger, S., Su, C.-W., and McMurtry, P.: Modeling entrainment and finescale mixing in cumulus
792 clouds, *J. Atmos. Sci.*, 54, 2697–2712, 1997.

793 Kumar, B., Schumacher, J., and Shaw, R. A.: Cloud microphysical effects of turbulent mixing and
794 entrainment, *Theor. Comput. Fluid Dyn.*, 27, 361–376, 2013.

795 Lasher-Trapp, S. G., Cooper, W. A., and Blyth, A. M.: Broadening of droplet size distributions
796 from entrainment and mixing in a cumulus cloud, *Q. J. Roy. Meteor. Soc.*, 131, 195–220, 2005.

797 Latham, J. and Reed, R. L.: Laboratory studies of the effects of mixing on the evolution of cloud
798 droplet spectra, *Q. J. Roy. Meteor. Soc.*, 103, 297–306, 1977.

799 Lehmann, K., Siebert, H., and Shaw, R. A.: Homogeneous and inhomogeneous mixing in cumulus
800 clouds: dependence on local turbulence structure, *J. Atmos. Sci.*, 66, 3641–3659, 2009.

801 Leon, D. C., French, J. R., Lasher-Trapp, S., Blyth, A. M., Abel, S. J., Ballard, S., Bennett, L. J.,
802 Bower, K., Brooks, B., Brown, P., Choullarton, T., Clark, P., Collier, C., Crosier, J., Cui, Z.,
803 Dufton, D., Eagle, C., Flynn, M. J., Gallagher, M., Hanley, K., Huang, Y., Kitchen, M.,
804 Korolev, A., Lean, H., Liu, Z., Marsham, J., Moser, D., Nicol, J., Norton, E. G., Plummer, D.
805 Price, J., Ricketts, H., Roberts, N., Rosenberg, P. D., Taylor, J. W., Williams, P. I., and Young,
806 G.: The Convective Precipitation Experiment (COPE): investigating the origins of heavy
807 precipitation in the southwestern UK, *B. Am. Meteorol. Soc.*, in press, 2016.

808 Lu, C., and Liu Y., Niu, S.: Examination of turbulent entrainment mixing mechanisms using a
809 combined approach. *J. Geoph. Res.*, 116, D20207, 2011.

810 Paluch, I. R.: Mixing and the droplet size spectrum: generalizations from the CCOPE data, *J.*
811 *Atmos. Sci.*, 43, 1984–1993, 1986.

812 Paluch, I. R. and Baumgardner, D. G.: Entrainment and fine-scale mixing in a continental
813 convective cloud, *J. Atmos. Sci.*, 46, 261–278, 1989.

814 Paluch, I. R. and Knight, C. A.: Mixing and evolution of cloud droplet size spectra in a vigorous
815 continental cumulus, *J. Atmos. Sci.*, 41, 1801–1815, 1984.

816 Pinsky, M., Khain, A., Korolev, A., and Magaritz-Ronen, L.: Theoretical investigation of mixing in
817 warm clouds – Part 2: Homogeneous mixing, *Atmos. Chem. Phys. Discuss.*, 15, 30269-30320,
818 doi:10.5194/acpd-15-30269-2015, 2015.

819 Pinsky, M., Khain, A., and Korolev, A.: Theoretical analysis of mixing in liquid clouds – Part 3:
820 Inhomogeneous mixing, *Atmos. Chem. Phys. Discuss.*, 15, 30321–30381, doi:10.5194/acpd-15-
821 30321-2015, 2015.

822 Rogers, R. R.: *A Short Course in Cloud Physics*, Pergamon press, Oxford, 227 pp., 1976.

823 Squires, P.: The growth of cloud drops by condensation. *Aust. J. Sci. Res.*, 5, 66–86, 1952.

824 Su, C.-W., Krueger, S. K., McMurtry, P. A., and Austin, P. H.: Linear eddy modeling of droplet
825 spectral evolution during entrainment and mixing in cumulus clouds, *Atmos. Res.*, 47-48, 41-58,
826 1998.

827 **Table 1**828 **List of Symbols**

Symbol	Description	Units
A_2	$\frac{pR_v}{e_s R_a} + \frac{L^2}{c_{pa} R_v T^2}$	-
a	$\frac{e_s R_a L^2}{p c_{pa} R_v T^2}$	-
b	$\frac{c_{pa} R_v T^2}{L^2}$	-
c_{pa}	specific heat capacity of dry air at constant pressure	$\text{J kg}^{-1}\text{K}^{-1}$
c_{pv}	specific heat capacity of water vapor at constant pressure	$\text{J kg}^{-1}\text{K}^{-1}$
\bar{D}	mean droplet diameter	m
D_2	mean square droplet diameter	m
D_v	mean volume droplet diameter	m
e	water vapor pressure	N m^{-2}
e_1	initial water vapor pressure in the cloud parcel	N m^{-2}
e_2	initial water vapor pressure in the entrained sub-saturated parcel	N m^{-2}
e_s	saturation vapor pressure above flat surface of water	N m^{-2}
$f(D)$	size distribution of cloud droplets normalized on unity	m^{-1}
L	latent heat for liquid water	J kg^{-1}
M_n	n -th moment of the droplet size distribution	$\frac{\int_0^\infty f(r)r^n dr}{\int_0^\infty f(r)dr}$ m^n
N	concentration of droplets	m^{-3}
N_1	concentration of droplets before mixing	m^{-3}
p	pressure of moist air	N m^{-2}
R_a	specific gas constant of moist air	$\text{J kg}^{-1}\text{K}^{-1}$
R_v	specific gas constant of water vapor	$\text{J kg}^{-1}\text{K}^{-1}$
RH	e/E_s , relative humidity over water (saturation ratio)	-

RH_1	initial relative humidity in the cloud volume ($RH_1=1$)	-
RH_2	relative humidity in the entrained sub-saturated parcel	-
RH_{m0}	relative humidity after instant mixing of cloudy and entrained air but before droplets evaporation	-
q	cloud liquid water mixing ratio (mass of liquid water per 1kg of dry air)	-
q_1	cloud liquid water mixing ratio before mixing	-
q_v	water vapor mixing ratio (mass of water vapor per 1kg of dry air)	-
S	$e/e_s - 1$, supersaturation	-
S_2	supersaturation of the dry out-of-cloud air	-
S_{m0}	supersaturation after instant mixing of cloudy and entrained air, but before droplets start evaporating	-
T	temperature	K
T_1	temperature of the cloud parcel before mixing	K
T_2	temperature of the entrained sub-saturated parcel before mixing	K
T_{m0}	temperature of the parcel after vapor mixing, but before droplet evaporation	K
β	extinction coefficient	m^{-1}
β_1	extinction coefficient before mixing	m^{-1}
δq_m	mixing ratio of liquid water required to saturate 1kg of the cloud volume after instant mixing, but before droplet evaporation.	-
δq^*	mixing ratio of liquid water required to saturate 1kg of the dry out-of-cloud air	-
μ	cloud fraction of mixing air, $0 \leq \mu \leq 1$	-
μ_{cr}	critical cloud fraction, such that for $\mu \leq \mu_{cr}$ all droplets evaporate	-
ρ_a	density of the dry air	$kg\ m^{-3}$
ρ_w	density of liquid water	$kg\ m^{-3}$
ξ	coefficient $0 \leq \xi \leq 1$ characterizing proximity of homogeneous mixing to inhomogeneous (when $\xi \rightarrow 0$).	-

830 **Figure Captions**

831 **Figure 1.** Classical conceptual diagram of (a) inhomogeneous and (b) homogeneous mixing. 1
832 initial state; 2 mixing state; 3 final state.

833 **Figure 2.** Dependence of critical mixing fraction μ_{cr} versus mixing ratio q_0 calculated from Eq.(7).
834 Circles indicate modeled points. The calculations were performed for $T=0C$ and
835 $H=3000m$.

836 **Figure 3.** Dependence of ξ versus μ . Numbers are the dimensionless ratios $\delta q^*/q_1$. Critical mixing
837 ratios μ_{cr} are indicated by stars. Grey area indicates area where the moments of
838 homogeneous and extreme inhomogeneous mixing may not be segregated from in-situ
839 measurements. Dashed line was calculated for the cloud in Figs.13-14.

840 **Figure 4.** Simulation of (a) liquid water mixing ratio, (b) droplet number concentration, (c) integral
841 droplet diameter, (d) extinction coefficient, (e) mean volume diameter, (f) time of phase
842 relaxation, (g) relative humidity in the mixed volume before droplet evaporation RH_{m0}
843 and at the equilibrium state RH_m , (h) final temperature T_{m0} versus ratio of mixing μ
844 formed after homogeneous and extreme inhomogeneous mixing between dry and cloudy
845 parcel with monodisperse droplets. Black stars indicate critical mixing fraction μ_{cr}
846 calculated from Eq.(7). The calculations were performed for $RH_2 = 0.2, 0.5, 0.8, 0.95$;
847 $D_1=20\mu m, N_1=500cm^{-3}; T_1 = T_2 = 0C; H=1000m$.

848 **Figure 5.** Dependence of normalized liquid water mixing ratio q/q_1 (a,d,g), extinction coefficient
849 β/β_1 (b,e,h) and mean volume diameter D_v/D_{v1} (c,f,j) versus normalized number
850 concentration N/N_1 for various humidity of the entrained air (a,b,c), for various liquid
851 water mixing ratios (d,e,f) and for various temperatures (g,h,j). The calculations were
852 performed the initial conditions: $H=1000m, D_1=20\mu m$; for (a-c; g-j) $N_1=500cm^{-3}$; for (a-f)
853 $T_1 = T_2 = 0C$.

854 **Figure 6.** Simulation of (a) droplet number concentration and (b) liquid water mixing ratio, (c)
855 integral droplet diameter, (d) extinction coefficient, (e) mean volume diameter, (f) time of
856 phase relaxation, (g) relative humidity in the mixed volume before droplet evaporation
857 RH_{m0} and at the equilibrium state RH_m , (h) final temperature T_m versus ratio of mixing μ
858 formed after homogeneous and extreme inhomogeneous mixing between dry and cloudy

859 parcel with monodisperse droplets. The calculations were performed for $RH_2=0.9$;
860 $D_1=10\mu\text{m}$, $N_1=500\text{cm}^{-3}$; $T_1=0\text{C}$; $T_2=-10\text{C}, -5\text{C}, 0\text{C}$; $H=1000\text{m}$.

861 **Figure 7.** Effect of temperature difference between cloud and entrained air on mixing. The
862 calculations were performed for initial temperatures T_2 : (1) -10C ; (2) -5C ; (3) 0C . Grey
863 circles indicate extremely inhomogeneous mixing on line 1 at the AB interval. The rest
864 cases on extremely inhomogeneous mixing are indicated by open circles. The initial
865 conditions used for the calculations were: $H=1000\text{m}$, $RH_2=90\%$; $D_1=10\mu\text{m}$, $N_1=500\text{cm}^{-3}$,
866 $T_1=0\text{C}$.

867 **Figure 8.** Conceptual diagram of cascade mixing of the out-of-cloud entrained parcel with the
868 cloudy environment

869 **Figure 9.** Simulation of stochastic mixing corresponding to stages 1-4 as indicated in Fig.8. Solid
870 red lines indicate the normalized dependences q , β , D_v vs. N for the primary stage of
871 homogeneous mixing. Dashed red lines indicate the same dependences for
872 inhomogeneous mixing. The initial conditions used for the simulations were: $H=1000\text{m}$,
873 $T_1=T_2=0\text{C}$; $RH_2=0.5$; $D_1=10\mu\text{m}$, $N_1=500\text{cm}^{-3}$.

874 **Figure 10.** Conceptual diagram explaining breaking the functional relationships between the
875 microphysical moment during progressive missing (see text).

876 **Figure 11.** Droplet size distributions formed during the progressive homogeneous mixing
877 corresponding to the (a,e) primary stage; (b,f) 2nd stage; (c,g) 3rd stage; (d,h) 4th stage. Left
878 column (a,b,c,d) corresponds to the case, when the cloud temperature is equal to the dry
879 air temperature $T_1=T_2=0\text{C}$.; right column (e,f,g,h) corresponds to the case when $T_1=$
880 0C , $T_2=-10\text{C}$. For both cases the simulation was performed for $D_1=10\mu\text{m}$; $N=500\text{cm}^{-3}$;
881 $RH_2=0.9$.

882 **Figure 12.** Conceptual diagrams of scattering of measurements of q versus N for (a) extreme
883 inhomogeneous and (b) homogeneous mixing.

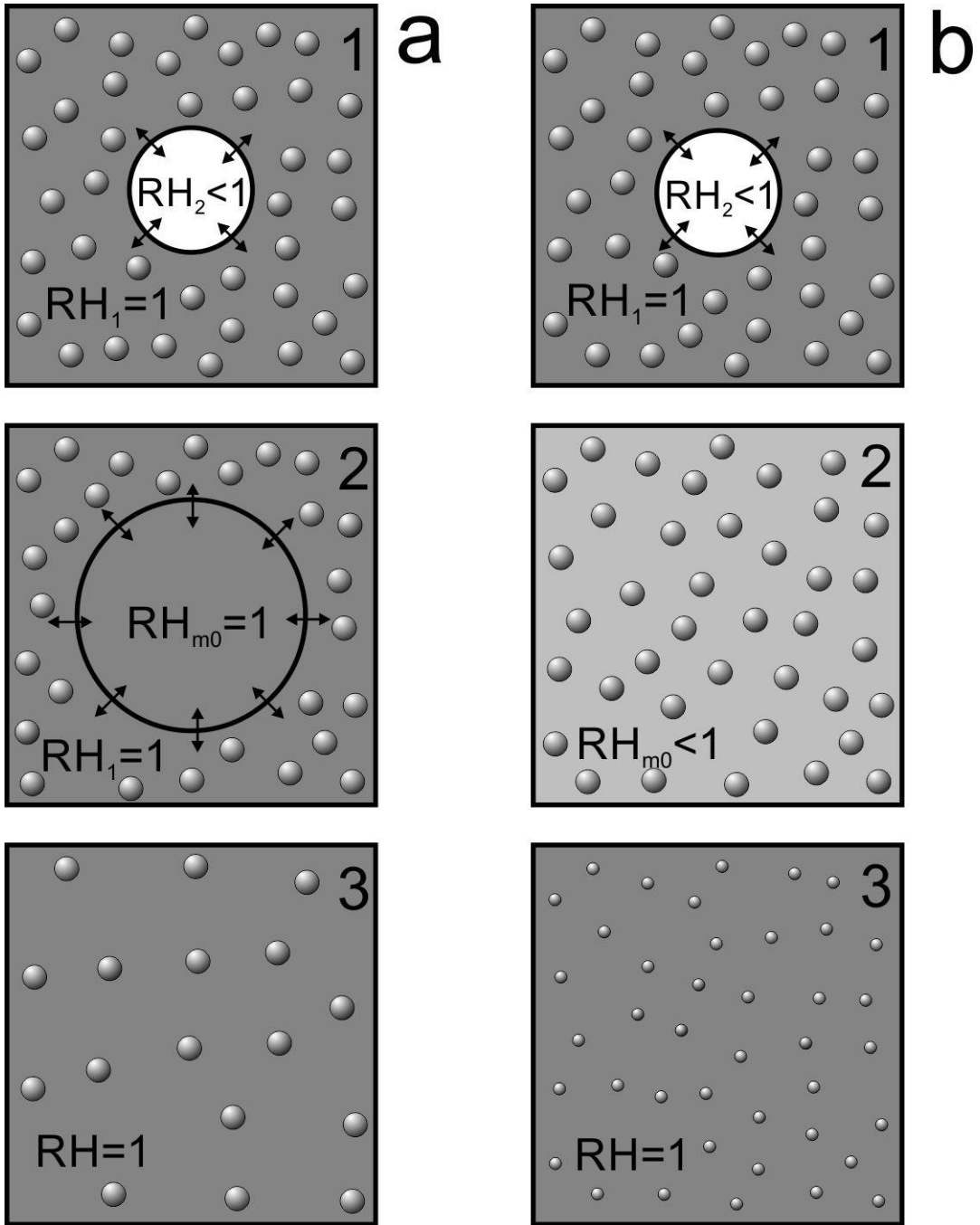
884 **Figure 13.** Spatial changes of particle concentration (a), extinction coefficient (b), liquid water
885 content (c) and average and mean mass diameter (d) during transit through one of the
886 convective clouds measured by CDP. The measurements were conducted during the
887 COPE-MED project on 18 July, 2015. The sampling rate 10Hz ($\sim 10\text{m}$ spatial resolution).
888 $H=5500\text{m}$, $T=-12\text{C}$, $RH=0.2$.

889 **Figure 14.** Relationships between (a) $LWC(N)$; (b) $\beta(N)$; (c) $D_v(N)$; (d) $LWC(\beta)$ calculated from
890 the CDP measurements obtained during sampling several convective clouds. The
891 measurements were conducted during the COPE-MED project on 18 July, 2015,
892 $H=5500\text{m}$, $T=-12\text{C}$, $RH=0.2$. The measurements were sampled at 10Hz ($\sim 10\text{m}$ spatial
893 resolution). Dashed lines are linear regressions. Red lines indicate primary
894 inhomogeneous mixing dependencies calculated for the same environmental conditions.

895 **Figure 15.** Relationships between (a) $LWC(N)$; (b) $\beta(N)$; (c) $D_v(N)$; (d) $LWC(\beta)$ calculated from
896 the CDP measurements sampled during traverse through 45 convective clouds. The
897 measurements were conducted during the COPE-MED project on 02 August, 2015.
898 Dashed lines indicate (a), (b) and (d) indicate the sectors, where the majority of the points
899 are scattered. The altitude of sampling varied in the range $3000\text{m} < H < 4500\text{m}$,
900 temperature $-11\text{C} < T < 0\text{C}$, relative humidity in the vicinity of clouds $15\% < RH < 65\%$. The
901 measurements were sampled at 10Hz ($\sim 10\text{m}$ spatial resolution).

902 **Figure A1.** Amount of evaporated liquid water δq_m required for saturation of a cloud volume with
903 initial humidity RH_m . Comparisons of the modeled δq_m and that calculated from Eqs.
904 (A8) and (A9) for three temperatures $T_{m0} = -20\text{C}$, 0C and 20C . Calculations were
905 performed for $P=880\text{mb}$.

906



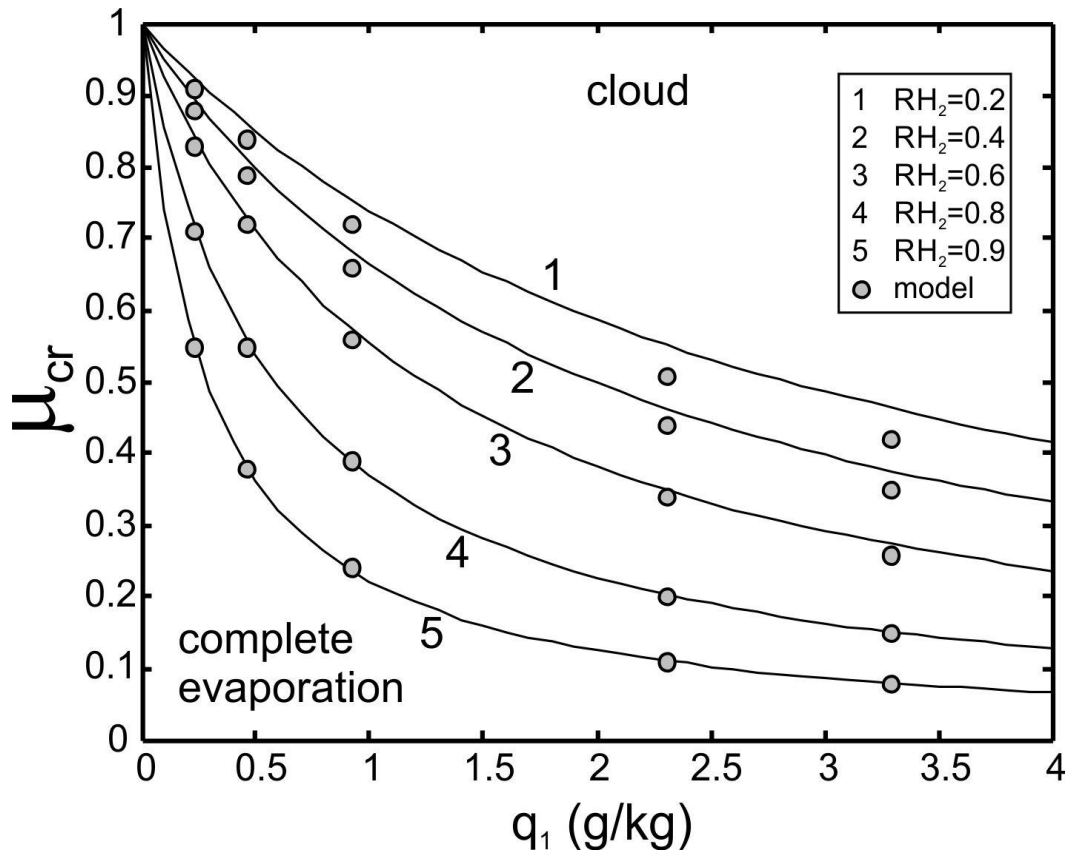
907

908

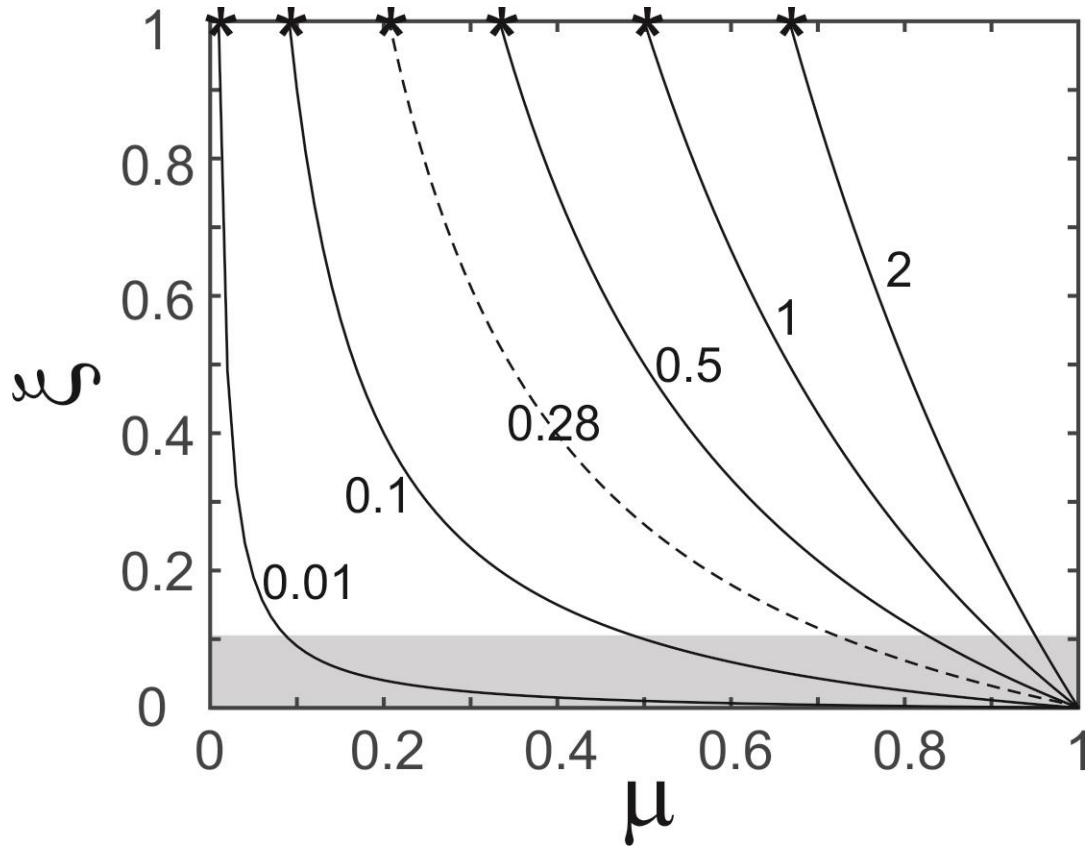
909 **Figure 1.** Classical conceptual diagram of (a) inhomogeneous and (b) homogeneous mixing. 1 initial state; 2
 910 mixing state; 3 final state.

911

912

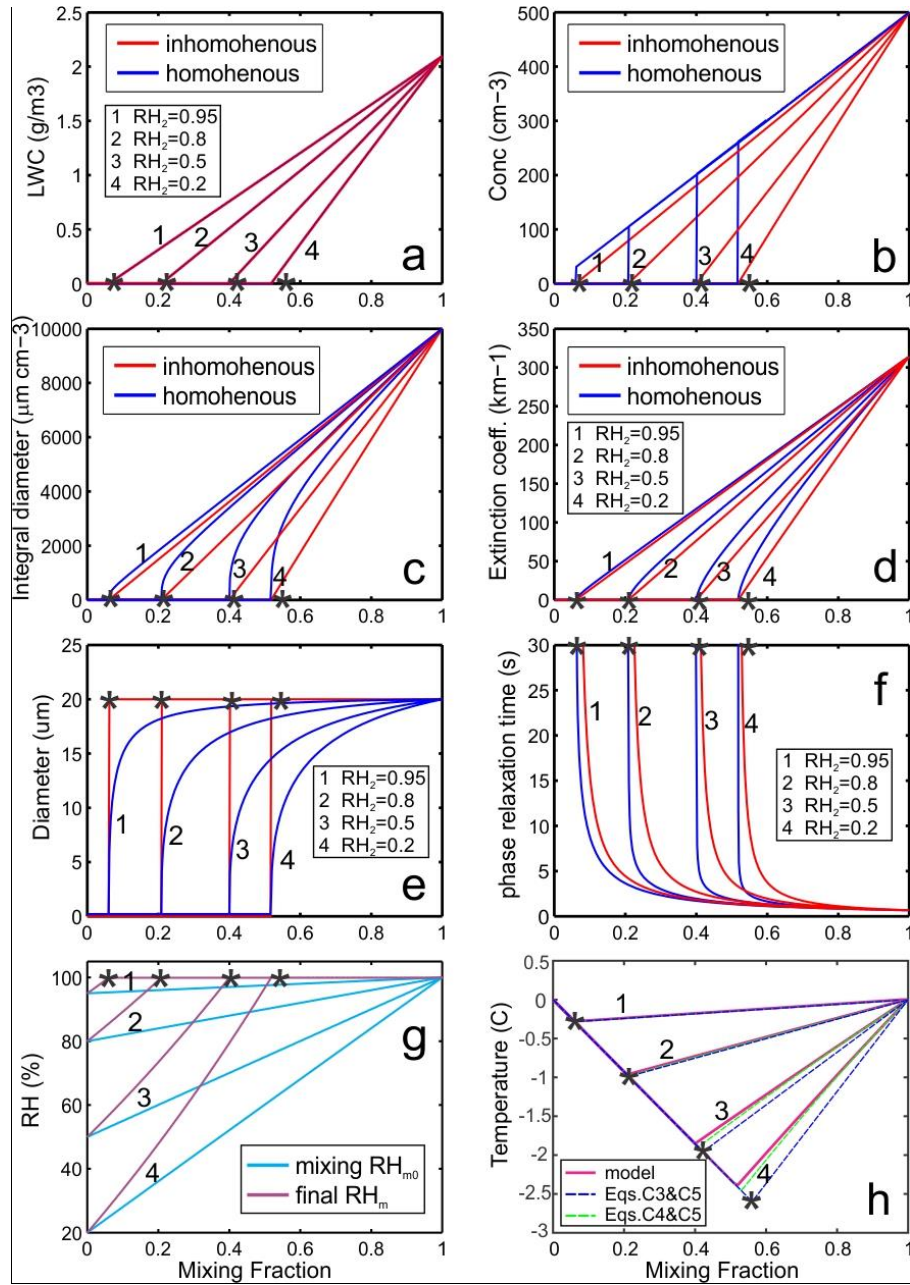


1
 2 **Figure 2.** Dependence of critical mixing fraction μ_{cr} versus mixing ratio q_0 calculated from Eq.(7).
 3 Circles indicate modeled points. The calculations were performed for $T=0C$ and $H=3000m$.
 4



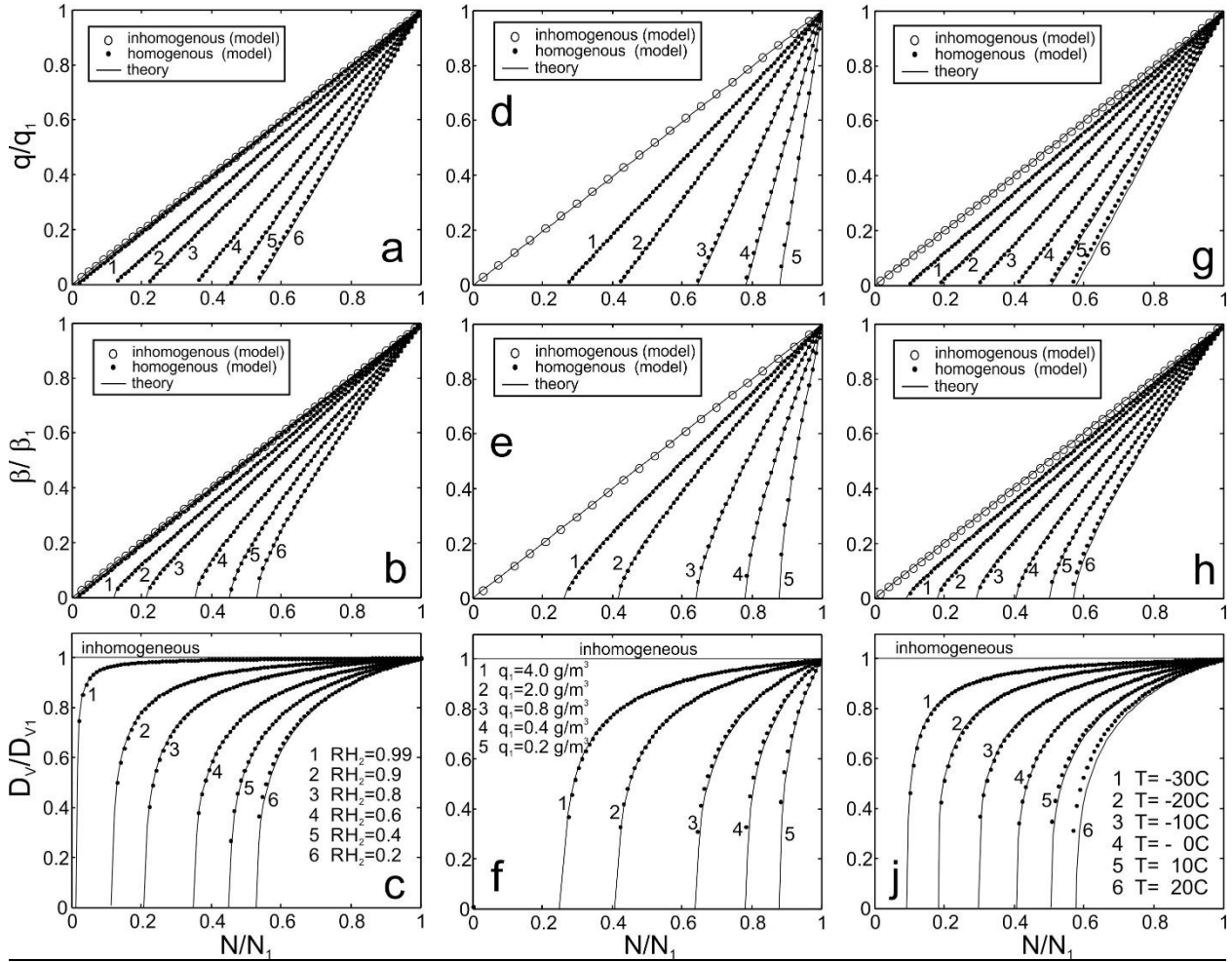
1
2
3
4
5
6
7

Figure 3. Dependence of ξ versus μ . Numbers are the dimensionless ratios $\delta q^*/q_1$. Critical mixing ratios μ_{cr} are indicated by stars. Grey area indicates area where the moments of homogeneous and extreme inhomogeneous mixing may not be segregated from in-situ measurements. Dashed line was calculated for the cloud in Figs.13-14.



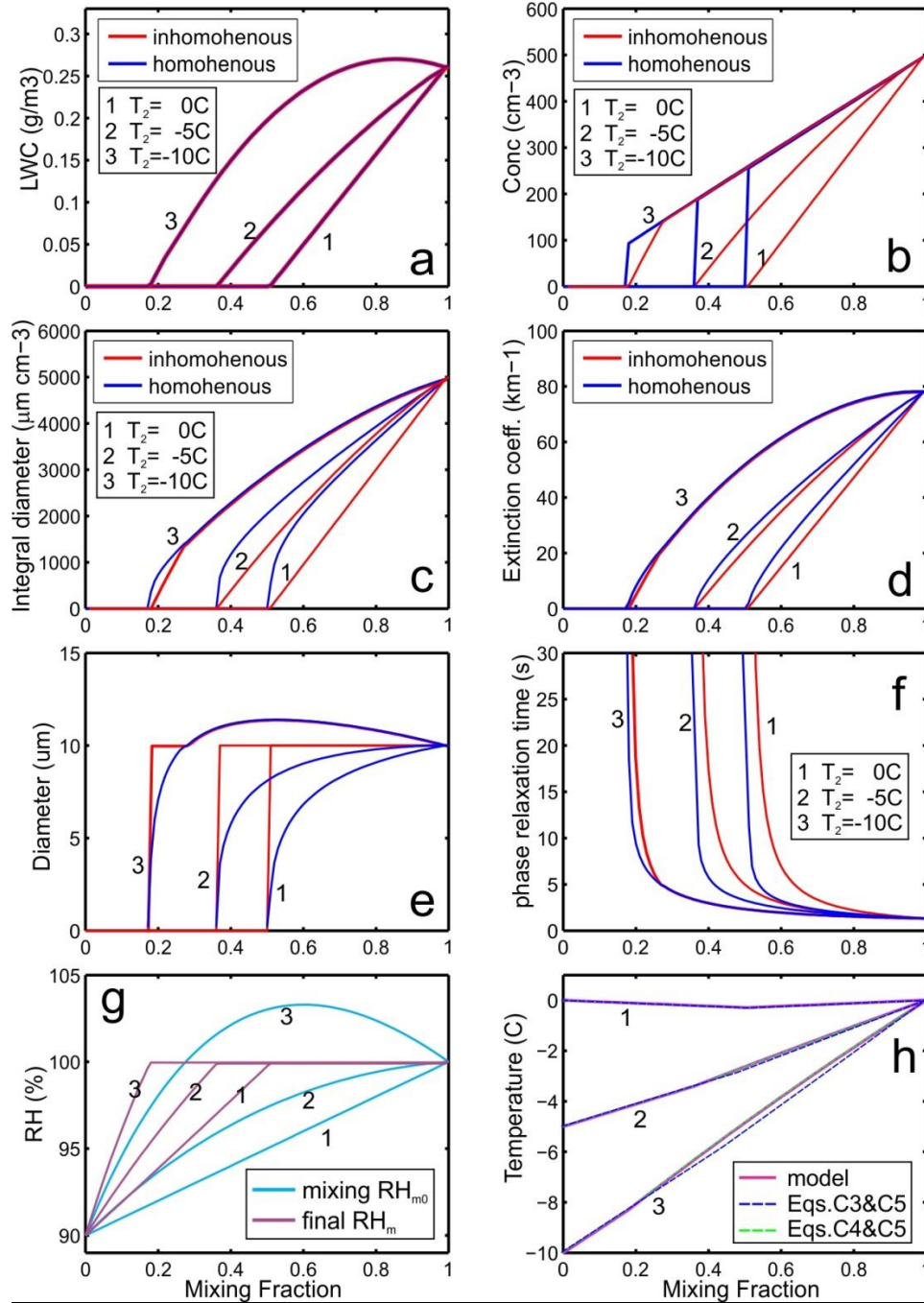
1
2

3 **Figure 4.** Simulation of (a) liquid water mixing ratio, (b) droplet number concentration, (c) integral
4 integral droplet diameter, (d) extinction coefficient, (e) mean volume diameter, (f) time of phase relaxation, (g)
5 relative humidity in the mixed volume before droplet evaporation RH_{m0} and at the equilibrium state
6 RH_m , (h) final temperature T_{m0} versus ratio of mixing μ formed after homogeneous and extreme
7 inhomogeneous mixing between dry and cloudy parcel with monodisperse droplets. Black stars indicate
8 critical mixing fraction μ_{cr} calculated from Eq.(7). The calculations were performed for $RH_2 = 0.2, 0.5,$
9 $0.8, 0.95; D_1=20\mu\text{m}, N_1=500\text{cm}^{-3}; T_1 = T_2 = 0\text{C}; H=1000\text{m}.$



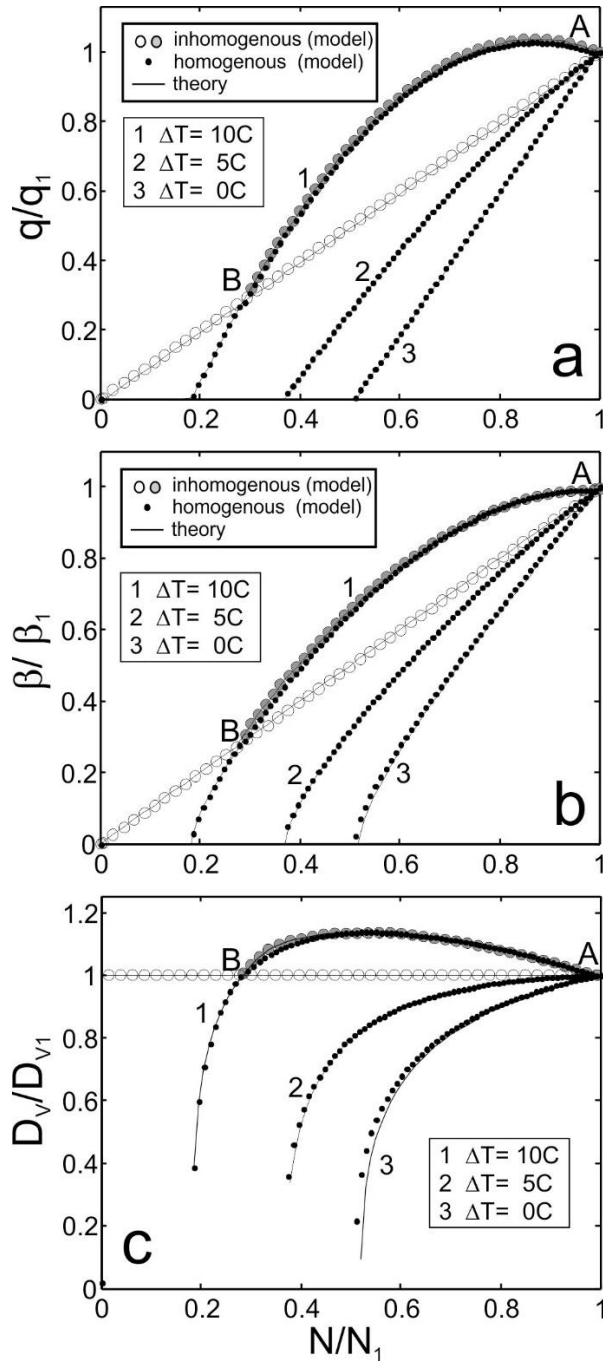
1
2
3 **Figure 5.** Dependence of normalized liquid water mixing ratio q/q_1 (a,d,g), extinction coefficient β/β_1
4 (β/β_1) (b,e,h) and mean volume diameter D_v/D_{v1} (c,f,j) versus normalized number concentration N/N_1 for
5 various humidity of the entrained air (a,b,c), for various liquid water mixing ratios (d,e,f) and for various
6 temperatures (g,h,j). The calculations were performed the initial conditions: $H=1000\text{m}$, $D_1=20\mu\text{m}$; for (a-
7 c; g-j) $N_1=500\text{cm}^{-3}$; for (a-f) $T_1 = T_2 = 0\text{C}$.

8



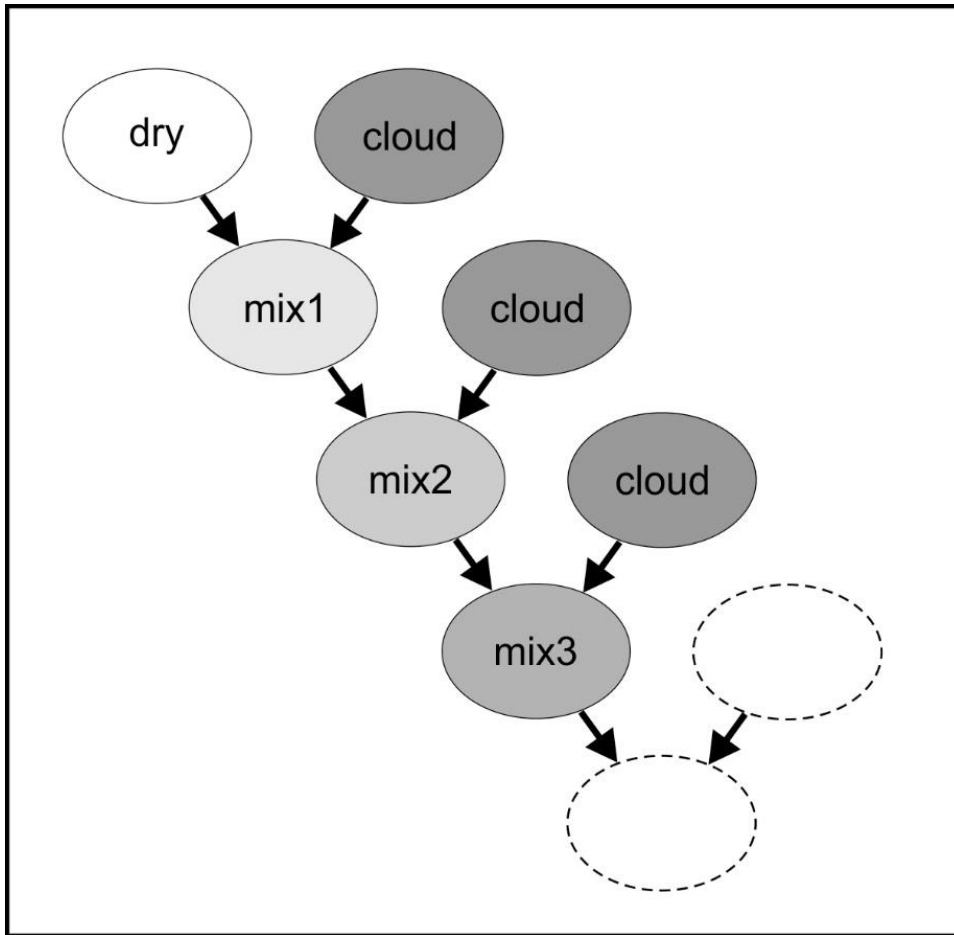
1
2

3 **Figure 6.** Simulation of (a) droplet number concentration and (b) liquid water mixing ratio, (c) integral
4 droplet diameter, (d) extinction coefficient, (e) mean volume diameter, (f) time of phase relaxation, (g)
5 relative humidity in the mixed volume before droplet evaporation RH_{m0} and at the equilibrium state
6 RH_m , (h) final temperature T_m versus ratio of mixing μ formed after homogeneous and extreme
7 inhomogeneous mixing between dry and cloudy parcel with monodisperse droplets. The calculations
8 were performed for $RH_2=0.9$; $D_1=10\mu\text{m}$, $N_1=500\text{cm}^{-3}$; $T_1 =0C$; $T_2 = -10C, -5C, 0C$; $H=1000\text{m}$.



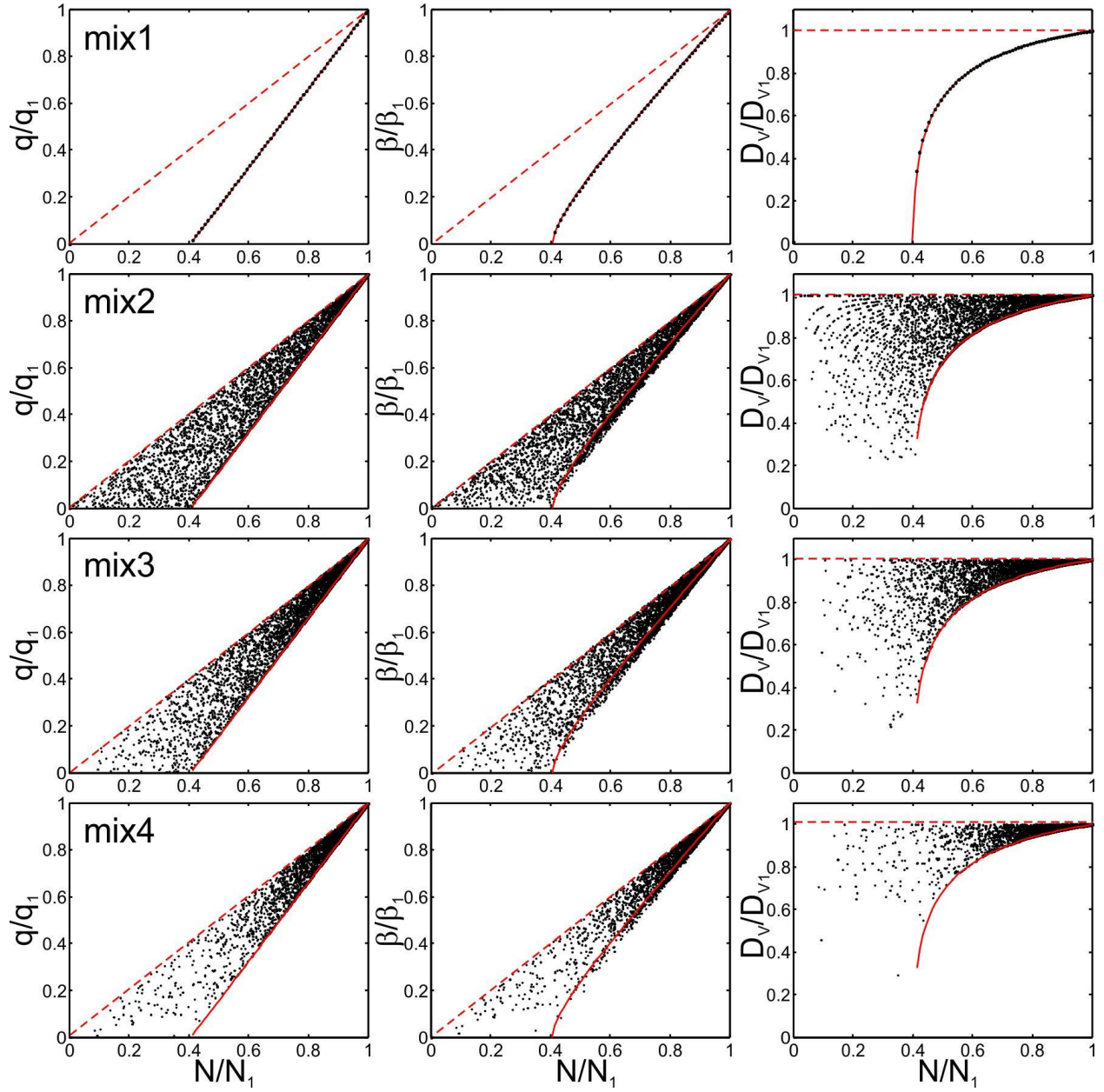
1
2

3 **Figure 7.** Effect of temperature difference between cloud and entrained air on mixing. The calculations
 4 were performed for initial temperatures T_2 : (1) -10C; (2) -5C; (3) 0C. Grey circles indicate extremely
 5 inhomogeneous mixing on line 1 at the AB interval. The rest cases on extremely inhomogeneous mixing
 6 are indicated by open circles. The initial conditions used for the calculations were: $H=1000\text{m}$, $RH_2=90\%$;
 7 $D_1 = 10\mu\text{m}$, $N_1 = 500\text{cm}^{-3}$, $T_1=0\text{C}$.



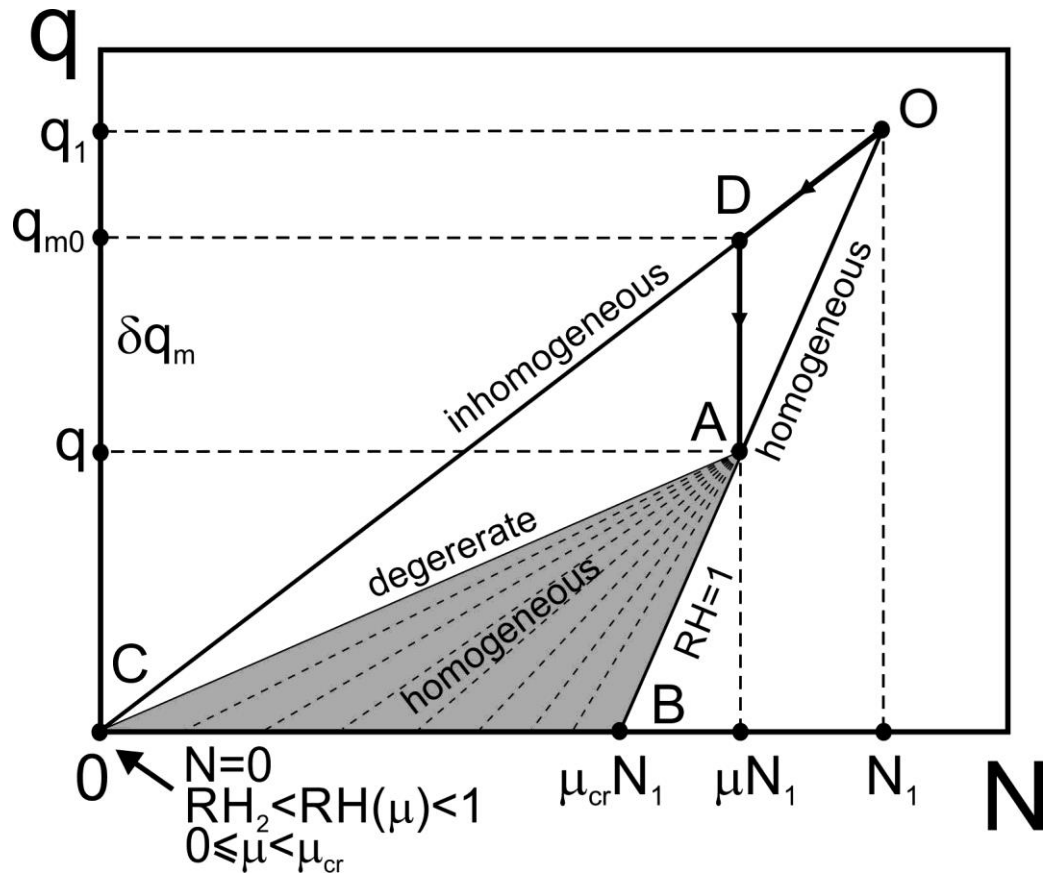
1
2
3
4
5
6

Figure 8. Conceptual diagram of cascade mixing of the out-of-cloud entrained parcel with the cloudy environment



7
8
9
10
11
12

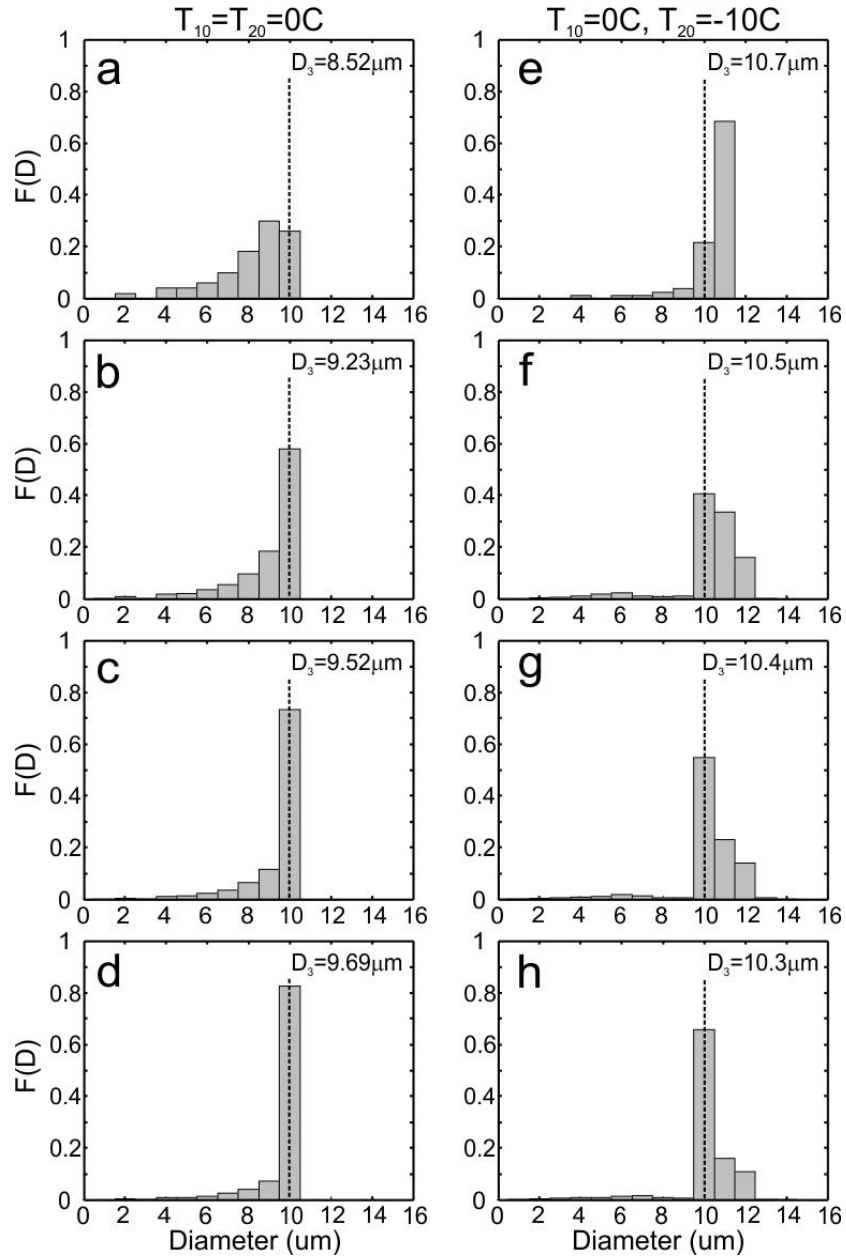
Figure 9. Simulation of stochastic mixing corresponding to stages 1-4 as indicated in Fig.8. Solid red lines indicate the normalized dependences q , β , D_v vs. N for the primary stage of homogeneous mixing. Dashed red lines indicate the same dependences for inhomogeneous mixing. The initial conditions used for the simulations were: $H=1000\text{m}$, $T_1 = T_2 = 0\text{C}$; $RH_2=0.5$; $D_1 = 10\mu\text{m}$, $N_1 = 500\text{cm}^{-3}$.



1
2
3
4
5

Figure 10. Conceptual diagram explaining breaking the functional relationships between the microphysical moment during progressive missing (see text).

1



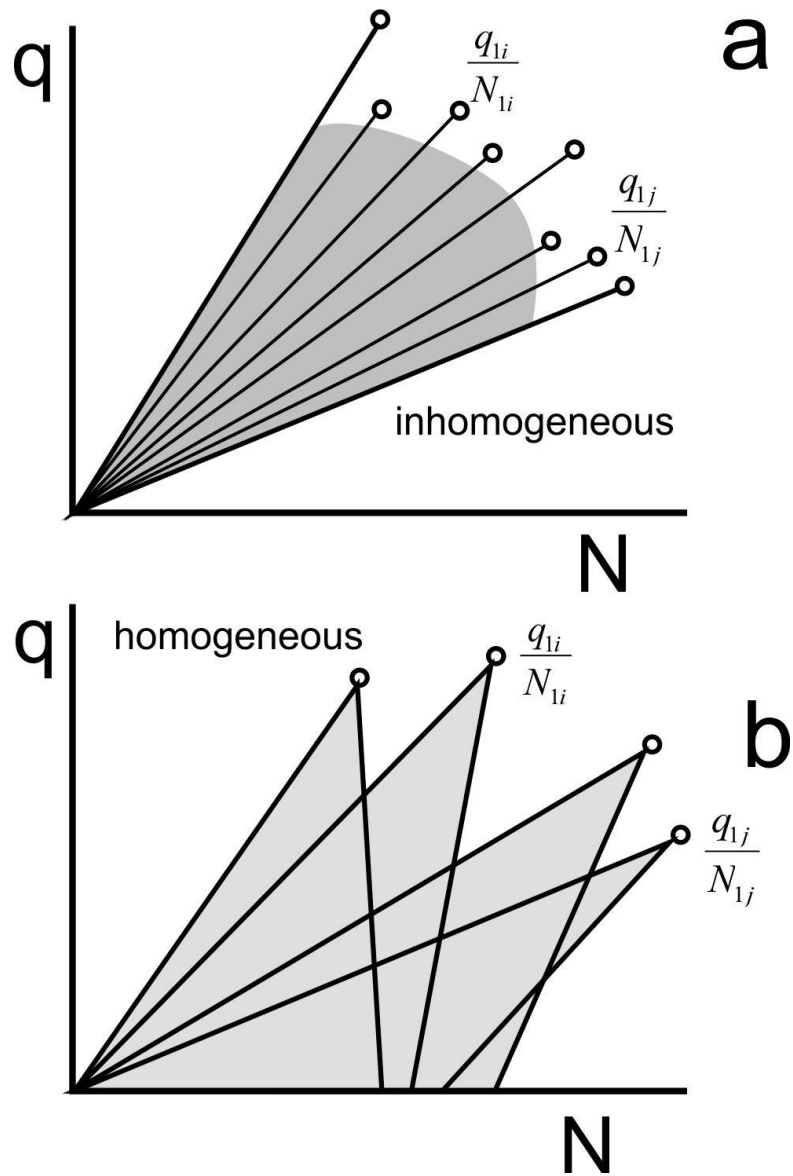
2

3

4 **Figure 11.** Droplet size distributions formed during the progressive homogeneous mixing corresponding
 5 to the (a,e) primary stage; (b,f) 2nd stage; (c,g) 3rd stage; (d,h) 4th stage. Left column (a,b,c,d) corresponds
 6 to the case, when the cloud temperature is equal to the dry air temperature $T_1 = T_2 = 0^\circ\text{C}$.; right column
 7 (e,f,g,h) corresponds to the case when $T_1 = 0^\circ\text{C}$, $T_2 = -10^\circ\text{C}$. For both cases the simulation was
 8 performed for $D_1 = 10\mu\text{m}$; $N=500\text{cm}^{-3}$; $RH_2=0.9$.

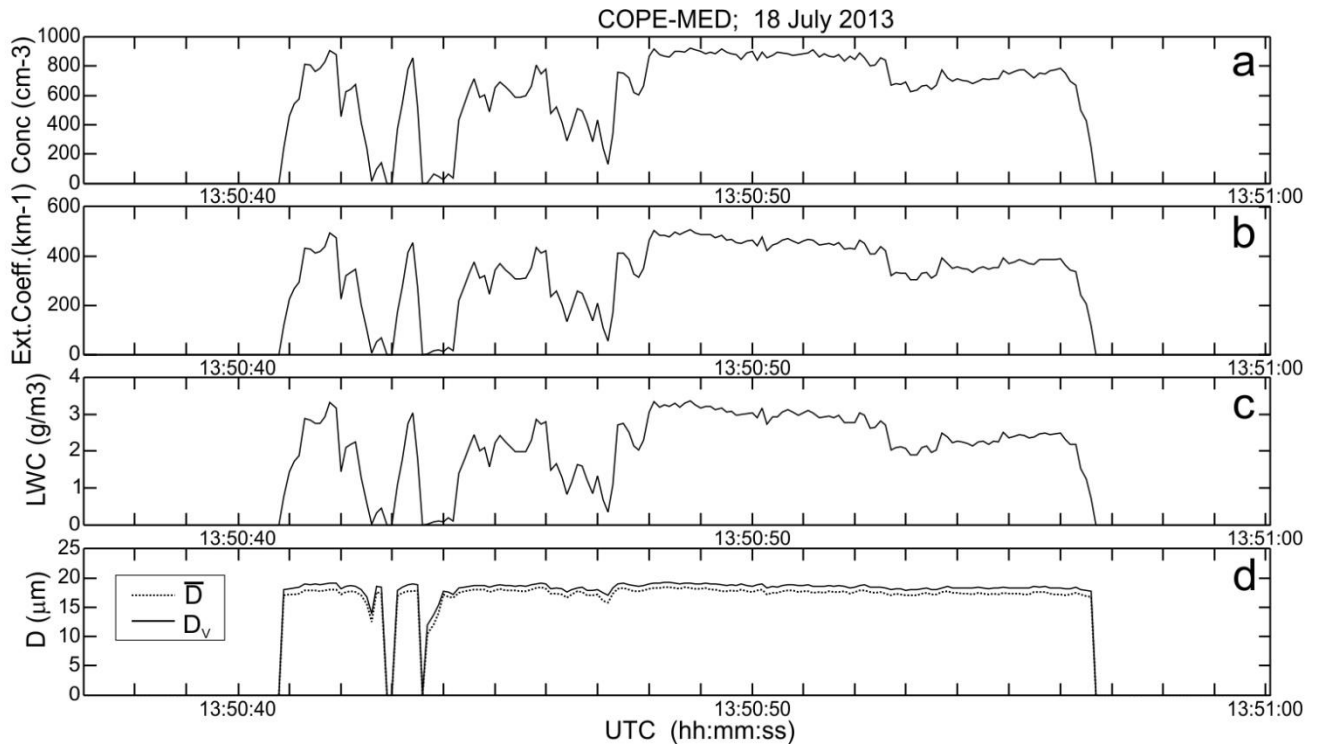
9

1
2



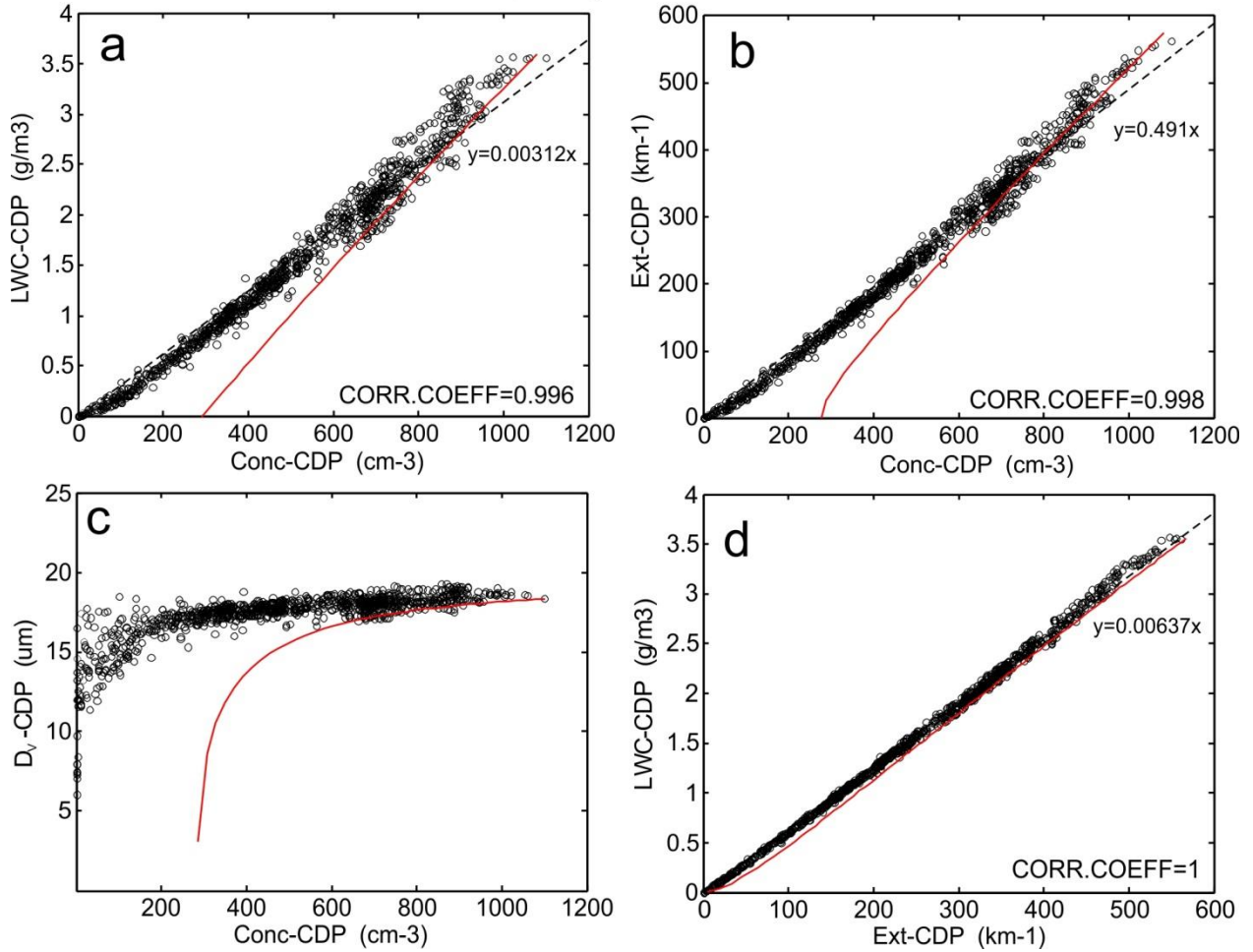
3
4
5
6
7
8

Figure 12. Conceptual diagrams of scattering of measurements of q versus N for (a) extreme inhomogeneous and (b) homogeneous mixing.



1
 2 **Figure 13.** Spatial changes of particle concentration (a), extinction coefficient (b), liquid water content
 3 (c) and average and mean mass diameter (d) during transit through one of the convective clouds measured
 4 by CDP. The measurements were conducted during the COPE-MED project on 18 July, 2015. The
 5 sampling rate 10Hz (~10m spatial resolution). $H=5500\text{m}$, $T=-12\text{C}$, $RH=0.2$.

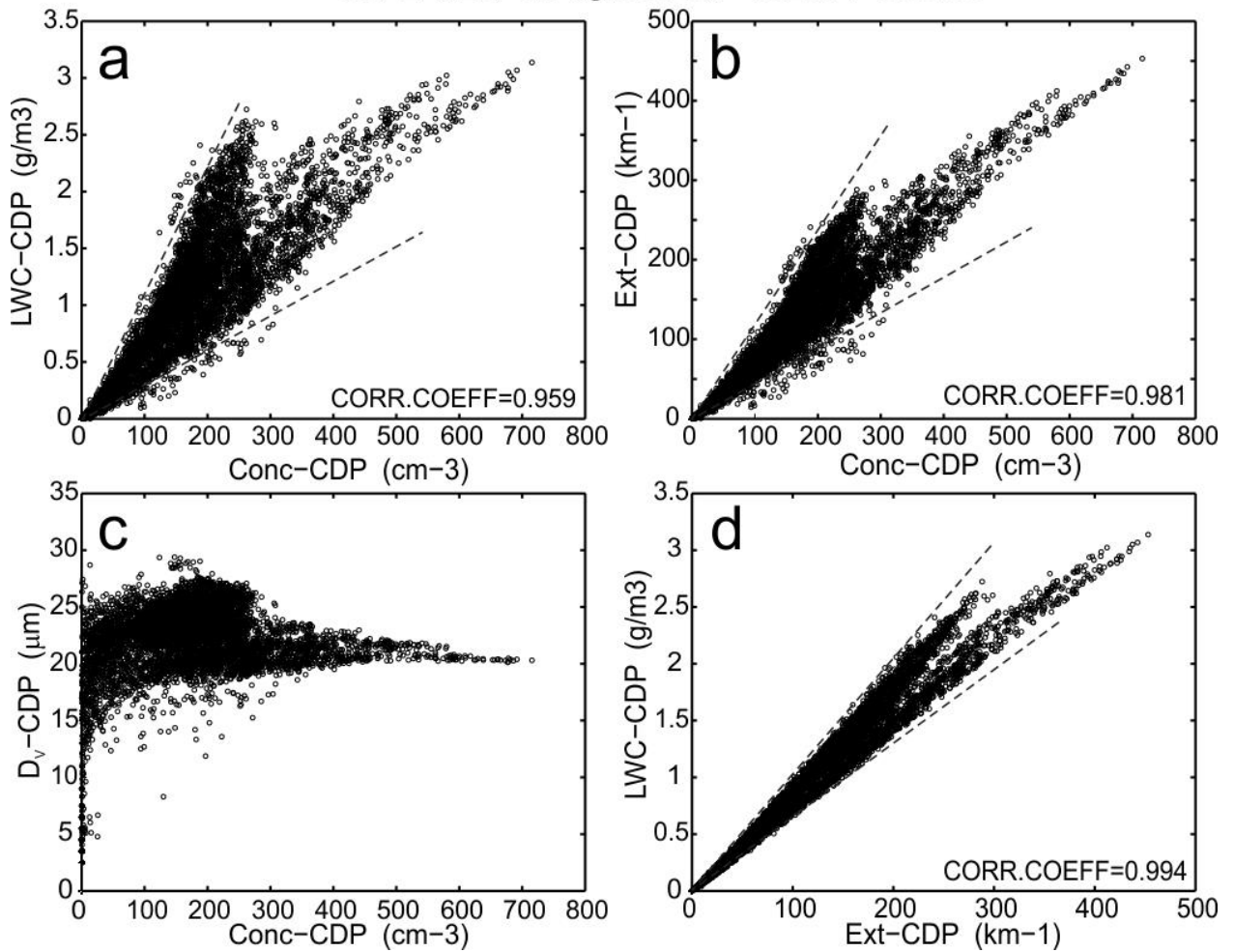
6



1
2
3
4
5
6
7
8
9
10

Figure 14. Relationships between (a) $LWC(N)$; (b) $\beta(N)$; (c) $D_v(N)$; (d) $LWC(\beta)$ calculated from the CDP measurements obtained during sampling several convective clouds. The measurements were conducted during the COPE-MED project on 18 July, 2015, $H=5500\text{m}$, $T=-12\text{C}$, $RH=0.2$. The measurements were sampled at 10Hz ($\sim 10\text{m}$ spatial resolution). Dashed lines are linear regressions. Red lines indicate primary inhomogeneous mixing dependencies calculated for the same environmental conditions.

COPE-MED; 02 August 2013; 13:25:01-15:38:06



1

2

3 **Figure 15.** Relationships between (a) $LWC(N)$; (b) $\beta(N)$; (c) $D_v(N)$; (d) $LWC(\beta)$ calculated from the
4 CDP measurements sampled during traverse through 45 convective clouds. The measurements were
5 conducted during the COPE-MED project on 02 August, 2015. Dashed lines indicate (a), (b) and (d)
6 indicate the sectors, where the majority of the points are scattered. The altitude of sampling varied in the
7 range $3000m < H < 4500m$, temperature $-11C < T < 0C$, relative humidity in the vicinity of clouds
8 $15% < RH < 65%$. The measurements were sampled at 10Hz ($\sim 10m$ spatial resolution).

9

10

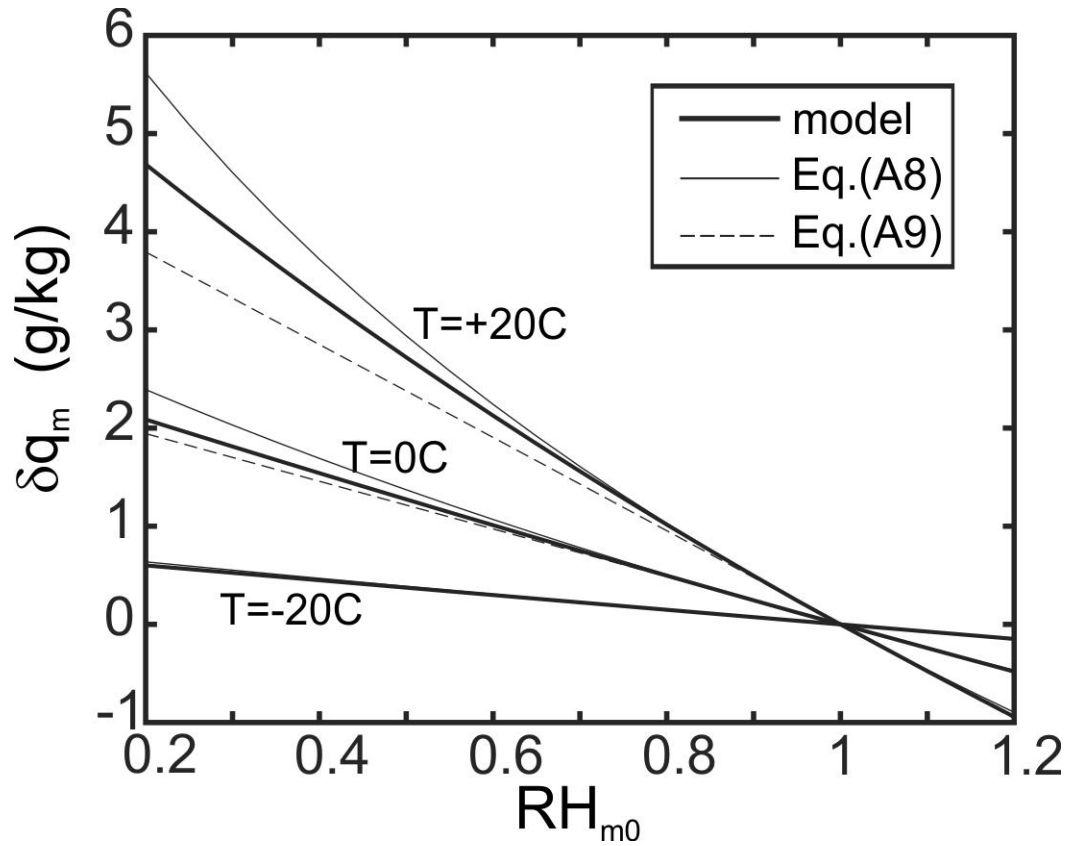


Figure A1. Amount of evaporated liquid water δq_m required for saturation of a cloud volume with initial humidity RH_m . Comparisons of the modeled δq_m and that calculated from Eqs. (A8) and (A9) for three temperatures $T_{m0} = -20C, 0C$ and $20C$. Calculations were performed for $P=880mb$.